Magnetic Materials for Energy

TECHNISCHE UNIVERSITÄT DARMSTADT

Fraunhofer ISC-IWKS

Permanent Magnets

Oliver Gutfleisch

Technical University of Darmstadt,
Material Science, Germany
and
Fraunhofer IWKS Hanau
Materials Recycling and Resource Strategy

- **Value chain**
- **Applications**
- **What makes a good magnet**
- **Coercivity mechanisms (μ vs nano crystalline)**
- **Enhancing remanence (texture and exchange spring magnets)**
- **Recycling**

Rare earth value chain

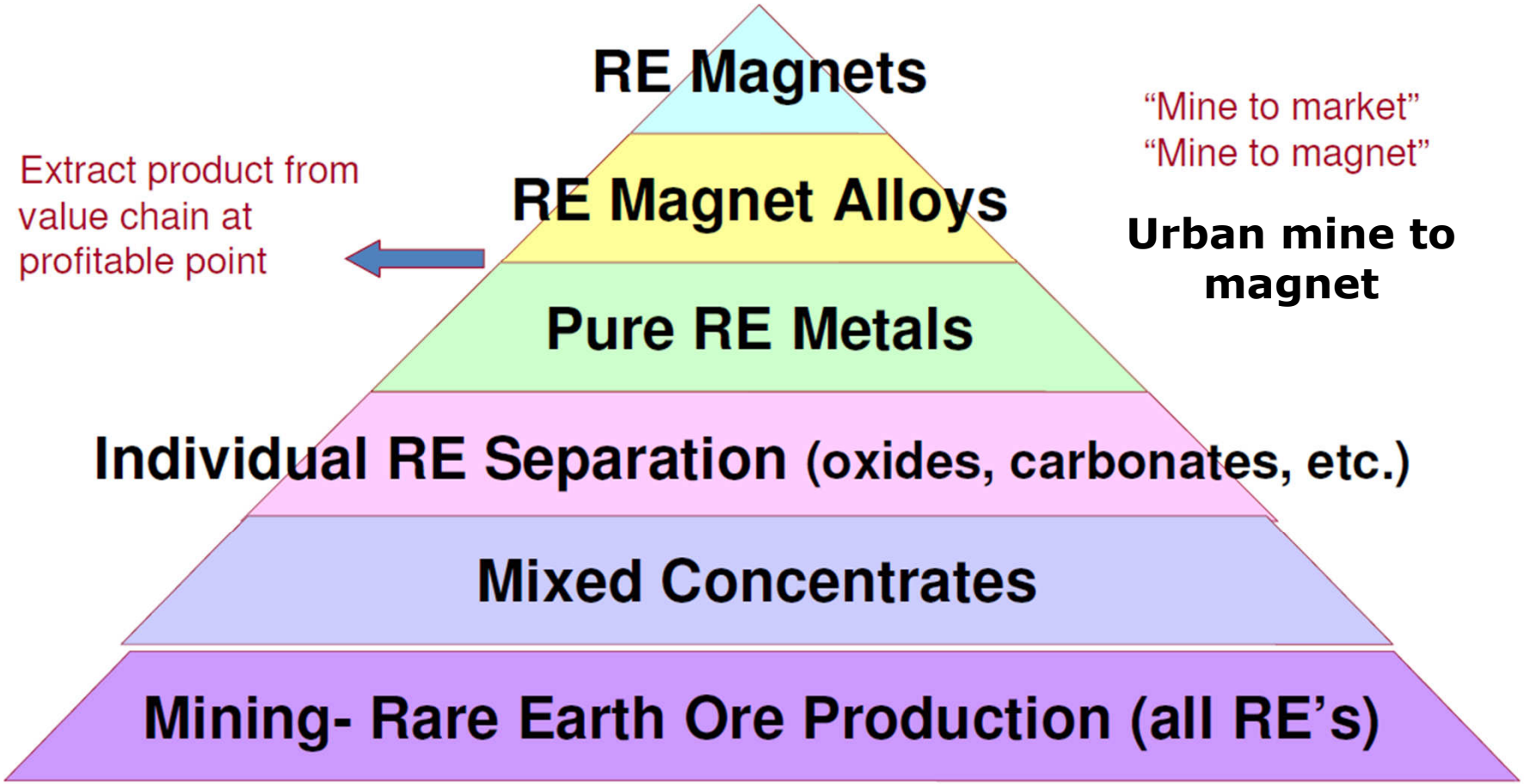

Courtesy P. Dent, MMM Conf. Nov. 2011

REs mining in China

Province / Region	2011 Mining Quota	
	LREOs (t)	HREOs (t)
Fujian	0	2,000
Guangdong	0	2,200
Guangxi	2,500	0
Hunan	1,500	0
Inner Mongolia	50,000	0
Jiangxi	0	9,000
Shandong	1,500	0
Sichuan	24,400	0
Yunnan	0	200
Sub-totals	80,400	13,400
Total Quota	93,800	
Actual Production	*96,900*	

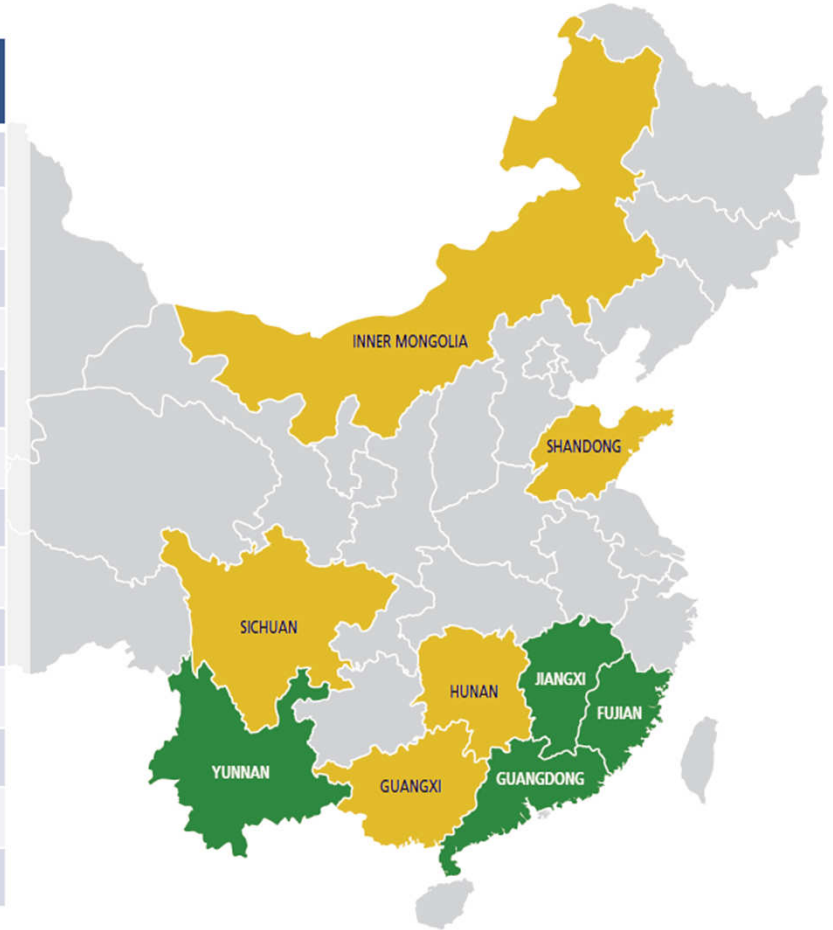

Sources: Technology Metals Research, Chinese Ministry of Land & Resources, Chinese State Council Information Office

Rare earth oxides in China

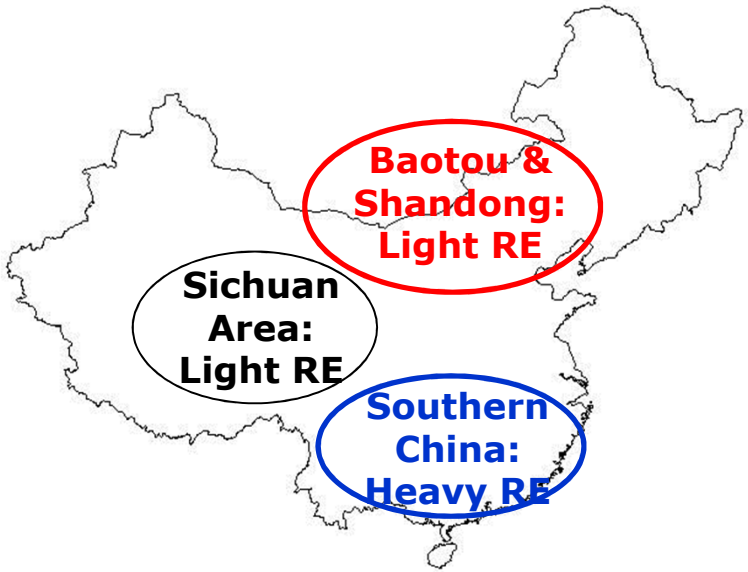

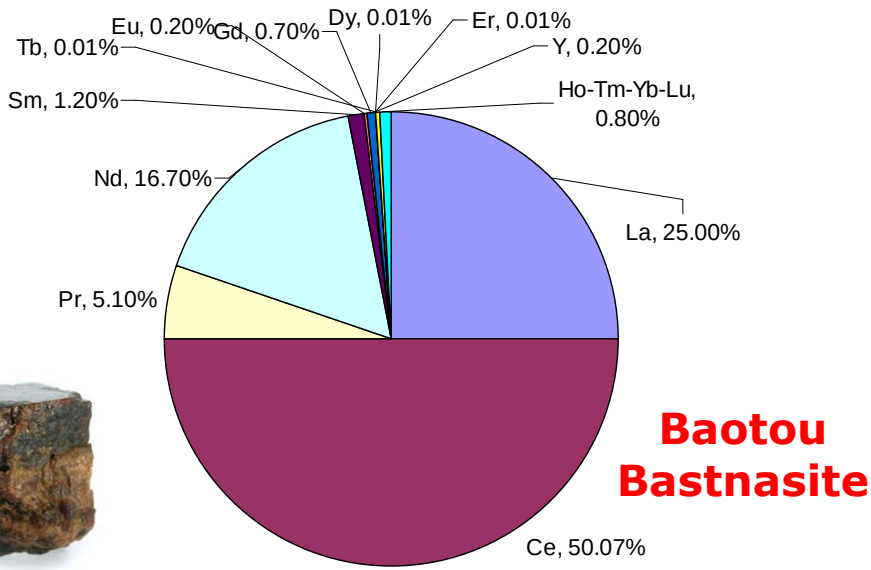

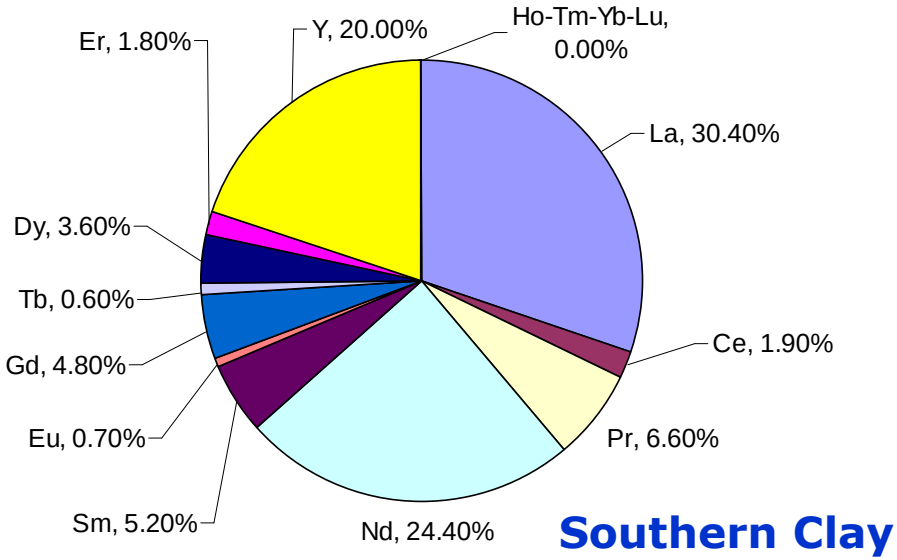

APPLICATIONS FOR PERMANENT MAGNETS

- **motors and generators** (stepping-, servomotors)
- **electroacoustics** (loudspeaker, transmitter)
- **hard disc drives** (positioning of read/write heads, VCM)
- **magnetic separation** (ore refinement, sewage treatment)
- **PM bearings** (centrifuges)
- **holding systems** (vibration damper for machine tools)
- **automotive engineering** (ABS, actuators)
- **magnetic couplings** (hermetic separation of different media)
- **measuring instruments** (pulse meters)
- **switches and relays** (Hall switches, revolution counters)
- **NMR analysis and MRI tomographs** (medical diagnostics)
- **beam guiding systems** (sputtering devices, wave tubes)
- magnetic **MEMS**

MOTORS AND ACTUATORS

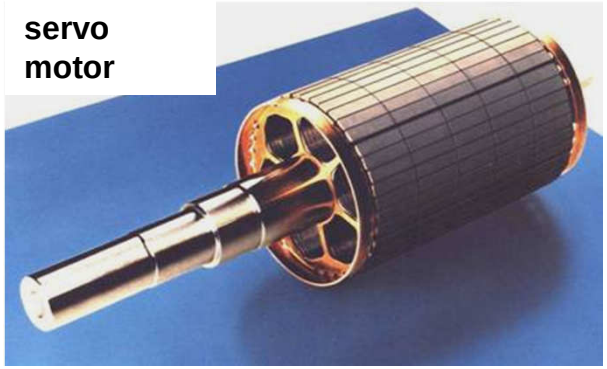

servo motor

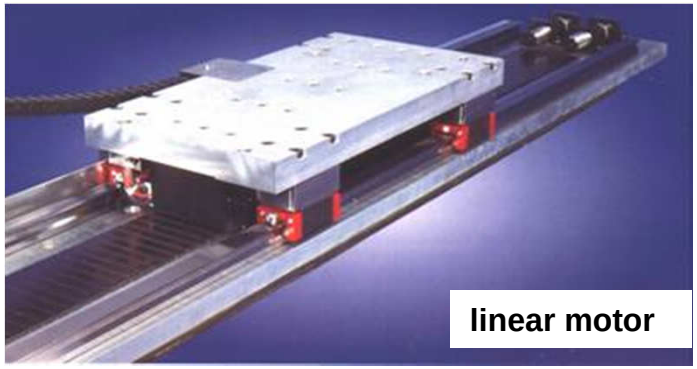

linear motor

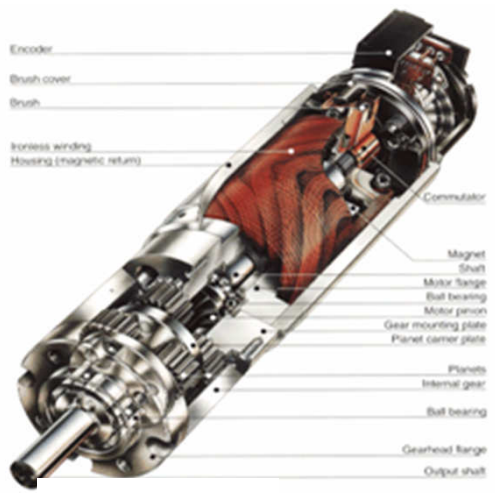

mini motor

Disk-Drive

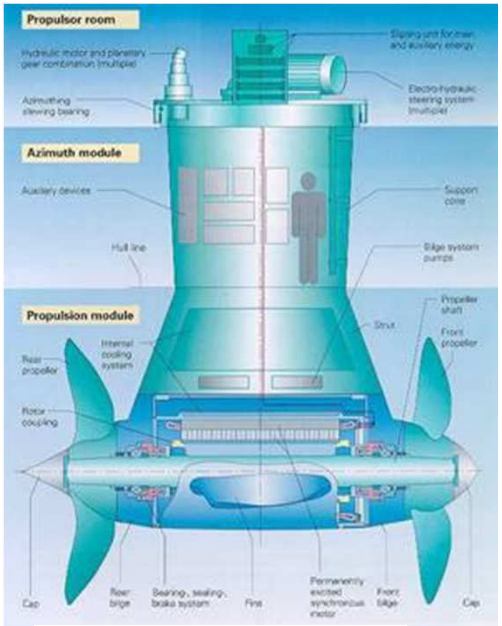

ship propulsion

TECHNISCHE UNIVERSITÄT DARMSTADT

AUTOMOBILE PARTS USING NDFEB MAGNETS

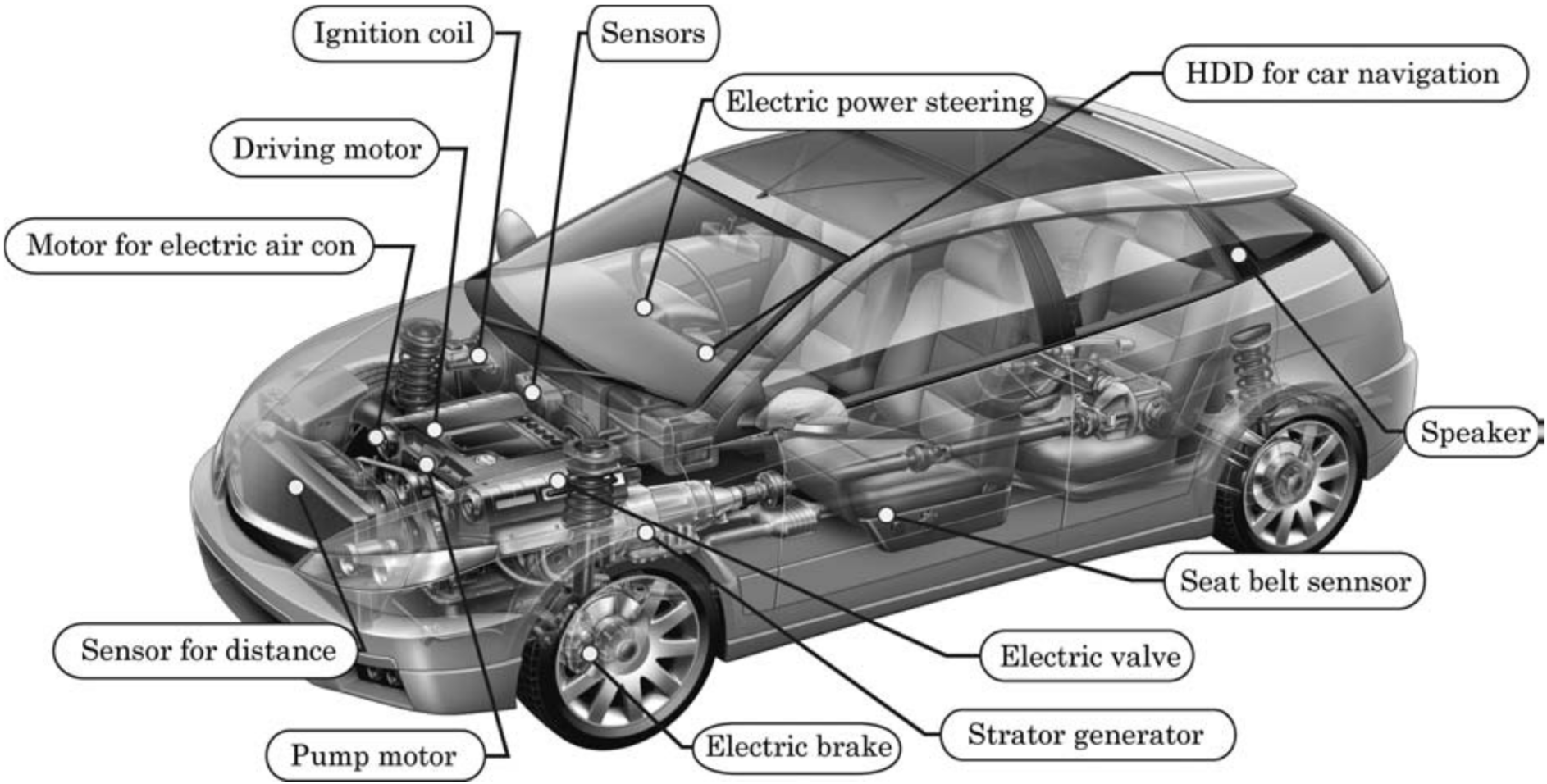

TECHNISCHE UNIVERSITÄT DARMSTADT

Permanent Magnet Growth

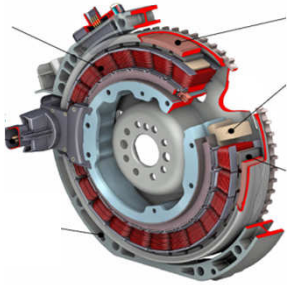

- **World production of sintered NdFeB in 2011: ~100.000 t (estimated 80% China, ~18% Japan, 2% Europe)**
- The **motor/generator in a hybrid electric vehicle contains 2 kg of NdFeB**. Set to grow to between 10 million and 20 million vehicles by 2018.
- New **designs of wind generators use NdFeB magnets at a rate of ~600 kg per mega-watt**. This application alone has potential to increase RE demand by 25% per year above current production.
- Hard disc drives cannot function without RE permanent magnets. Formerly 70% of the NdFeB market this is now diluted by the other major applications.
- Solid state energy efficient cooling: **Magnetocalorics 1kg MCE and 4 kg NdFeB per kilo-watt cooling power**

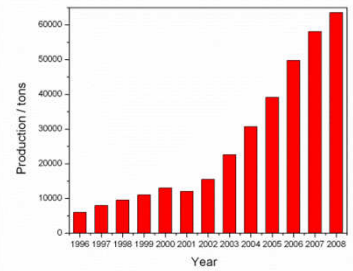

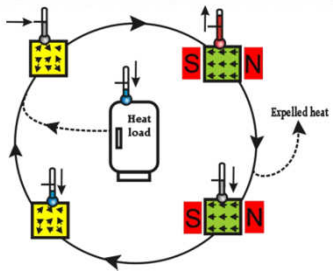

***Adv. Mat. (Review)* 23 (2011) 821**

Hysteresis Loop for Permanent Magnets

$(BH)_{max} = B_r^2/4\mu_0$

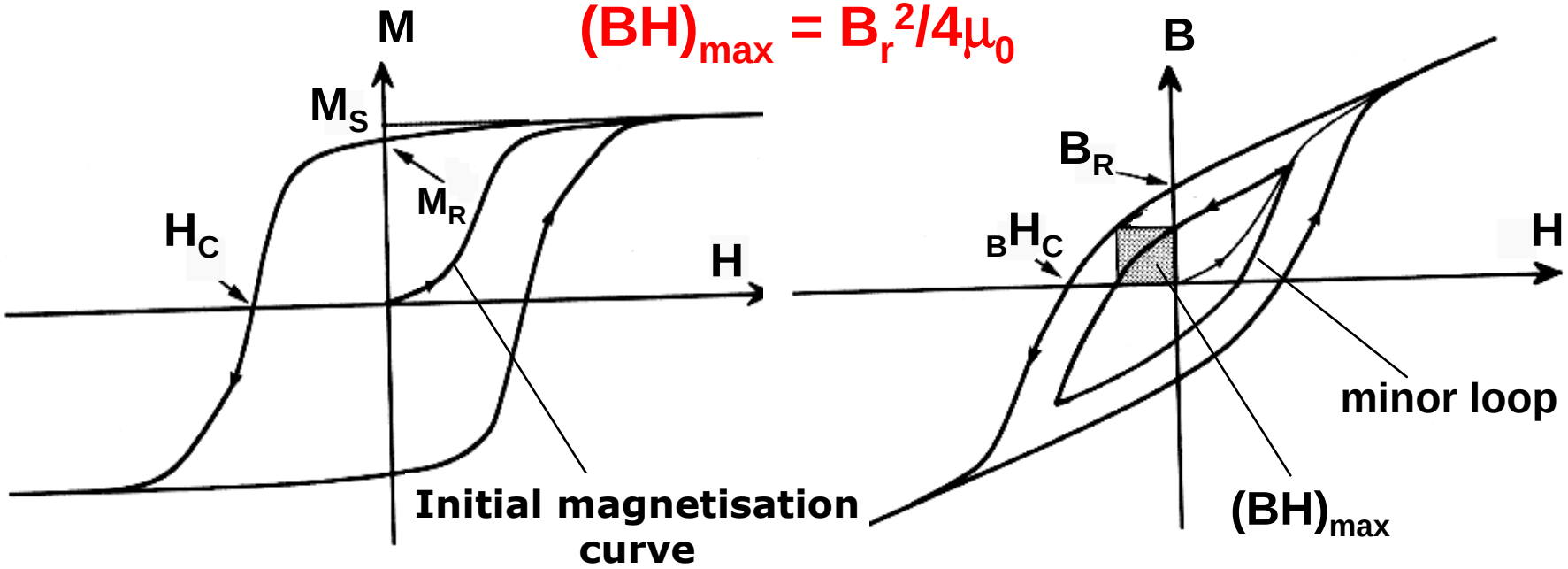

M-H loop

B-H loop

The initial magnetization curve after thermal demagnetization starts at the origin, a minor loop arising after the application of fields insufficient for saturation is also shown. The energy product $(BH)_{max}$ is the shaded area in the second quadrant of the B-H loop.

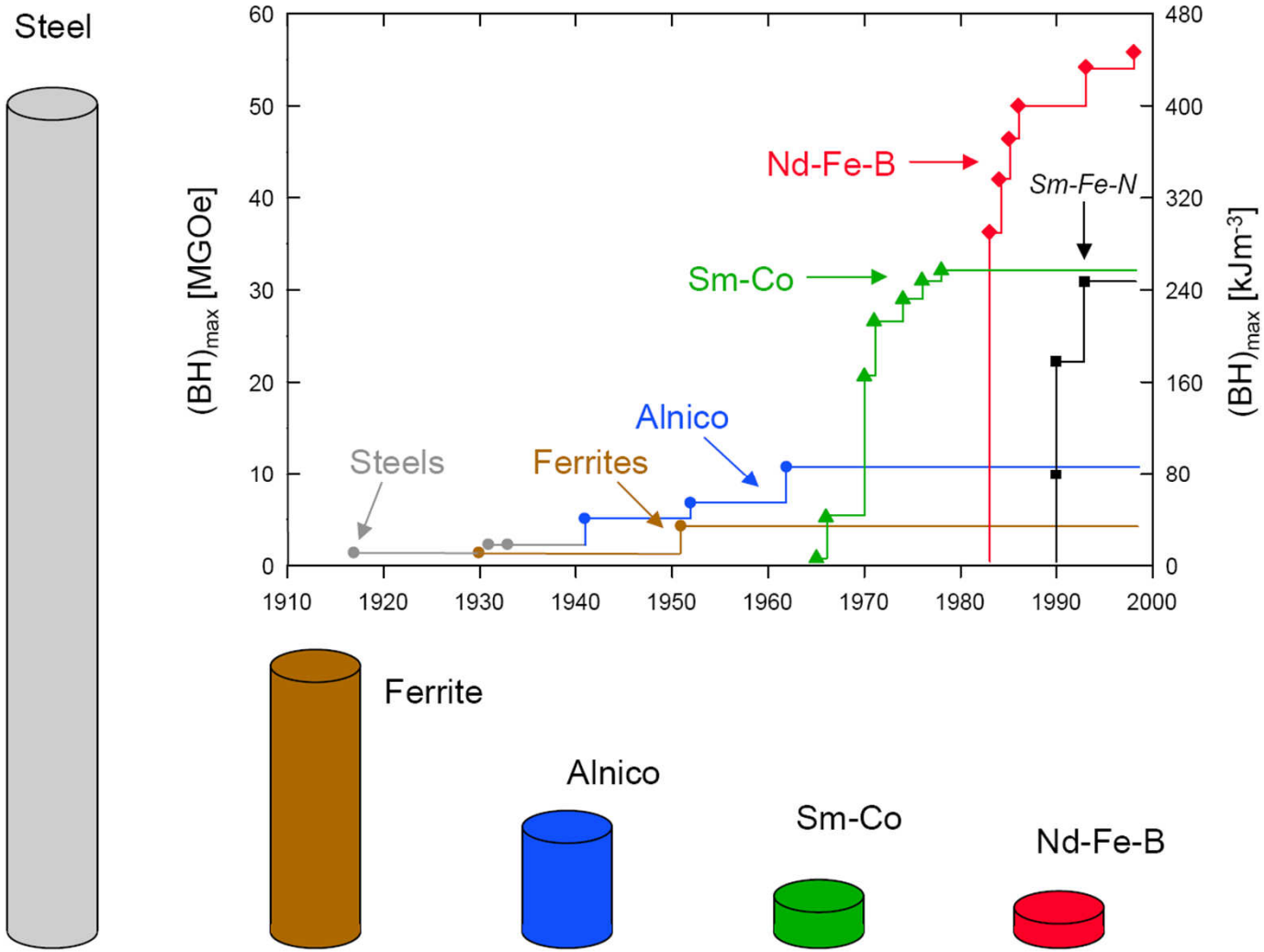

Adv. Mat. (Review) 23 (2011) 821

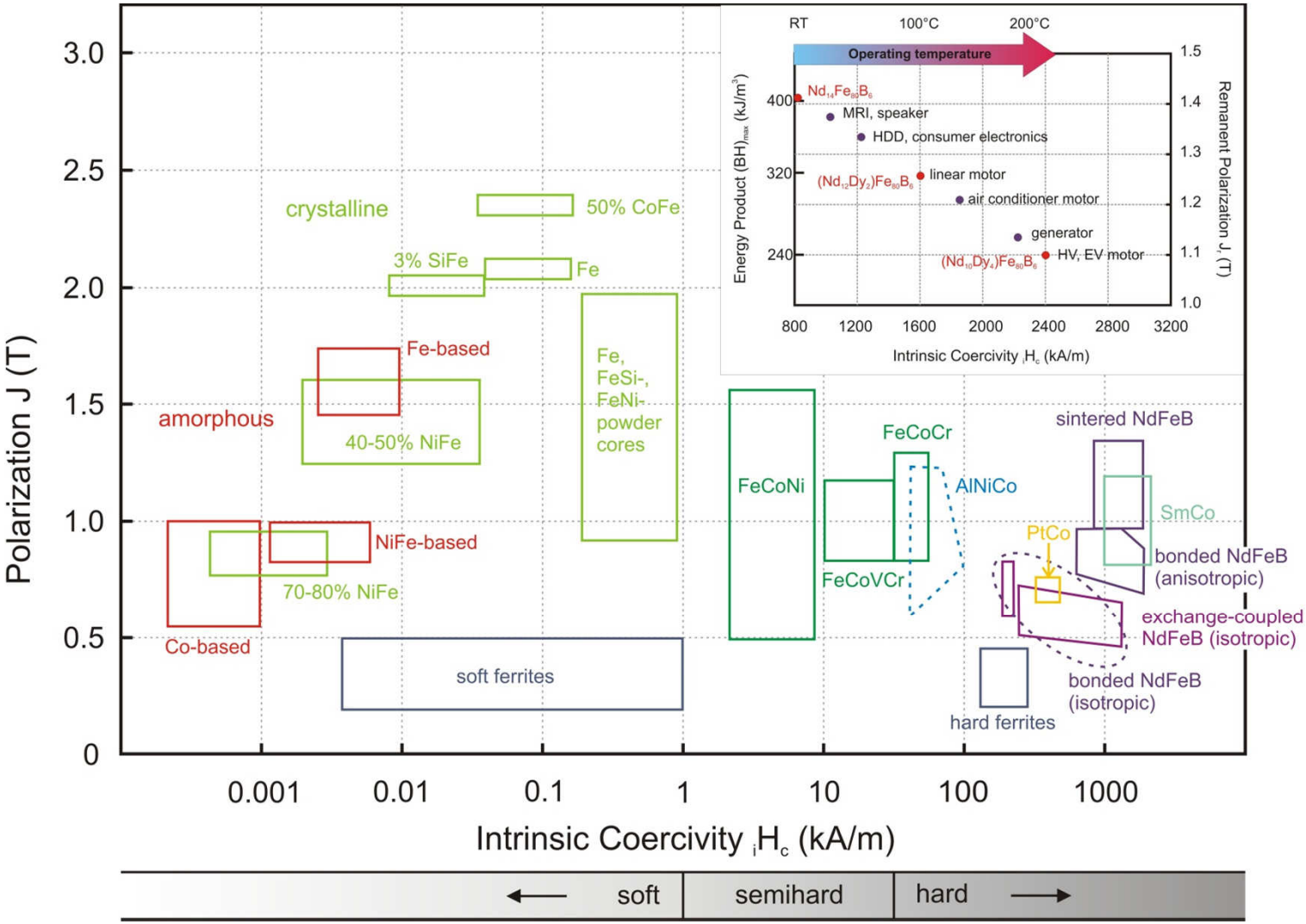

Adv. Mat. (Review) 23 (2011) 821

Sintered NdFeB magnets for electro motors

Design light-weight, high torque-to-weight ratio motors and generators, using PMs with adequate temperature stability

→ torque scales linearly with remanence

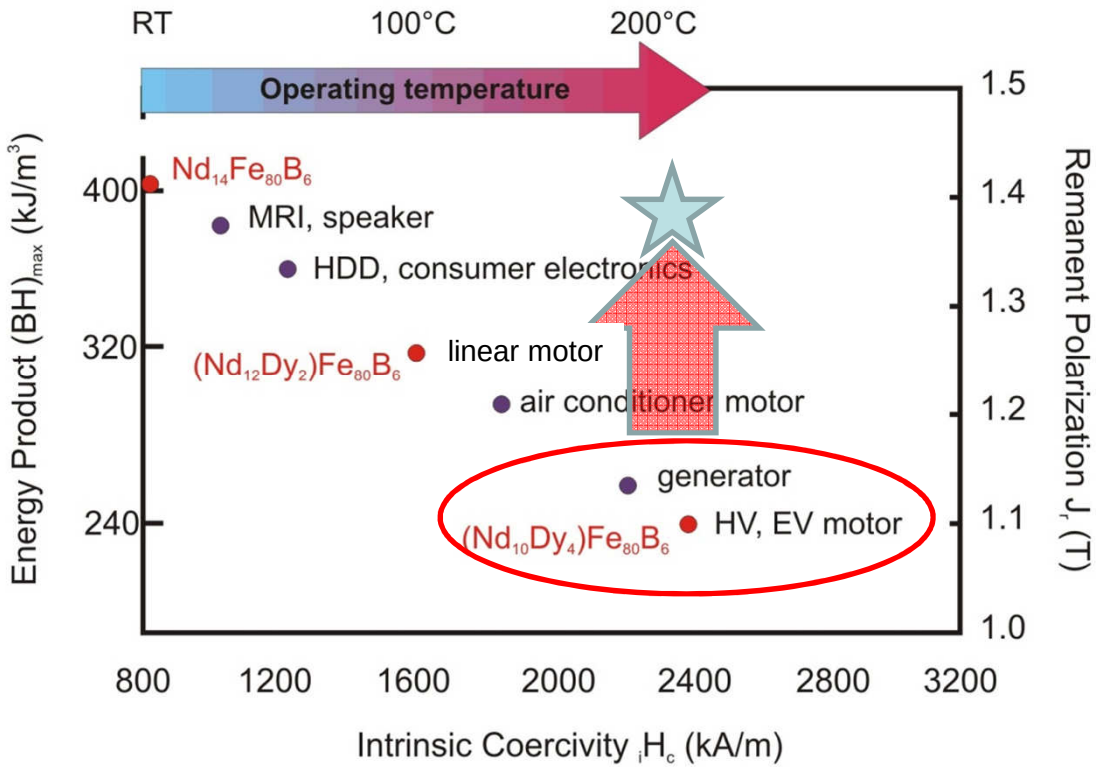

30 wt.% REE in a sintered magnet
(4-8 wt.% are heavy REEs Dy / Tb)

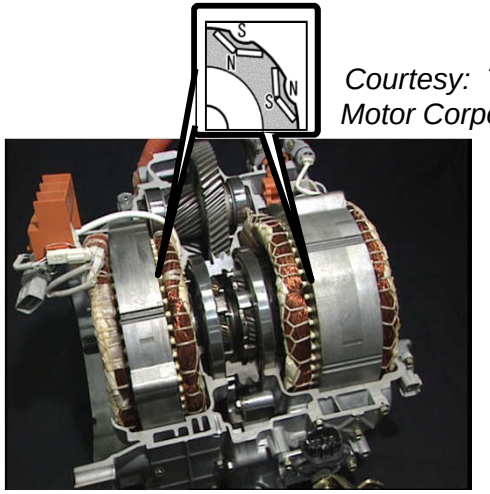

Courtesy: Toyota Motor Corporation

Courtesy: Siemens

***Adv. Mat.* 23 (2011) 821**

Intrinsic and extrinsic magnetic properties

intrinsic properties + **microstructure** **100µm > l > 1nm** **↔ fit µ-magnetic length scales** ⇒ **extrinsic properties**

saturation polarisation, J_s

anisotropy field, H_a

Curie temperature, T_C

remanence, J_r

coercivity, H_c

energy density, $(BH)_{max}$

compound	T_C , K	$\mu_0 M_s$, T	K_1, MJ/m³	d_c, nm	δ_w
$Nd_2Fe_{14}B$	585	1.60	5	214	4
$SmCo_5$	993	1.05	17	1700	3.7
Sm_2Co_{17}	1100	1.30	3.3	490	8.6
α-Fe	1043	2.16	0.046*	7	30

d_c: critical single-domain particle size

δ_w: domain wall width

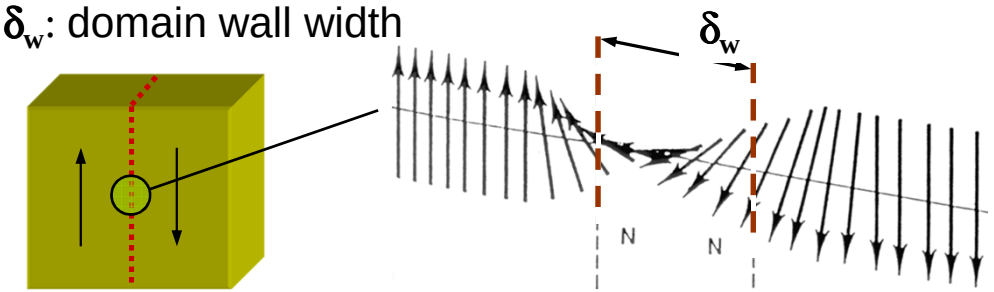

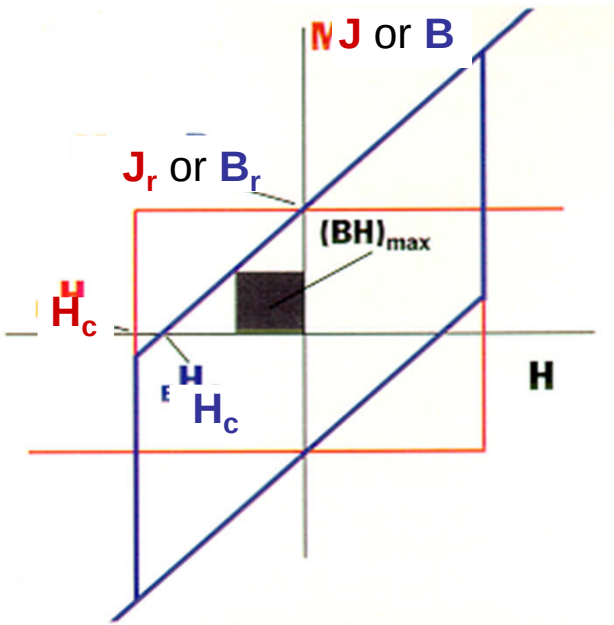

J. Phys. D: Appl. Phys. ***33*** *(2000) R157-R172*

Magnetism in $Nd_2Fe_{14}B$

Element	M_S	K_1	T_C
Fe 3d	high	low	high
Nd 4f	low	high	low

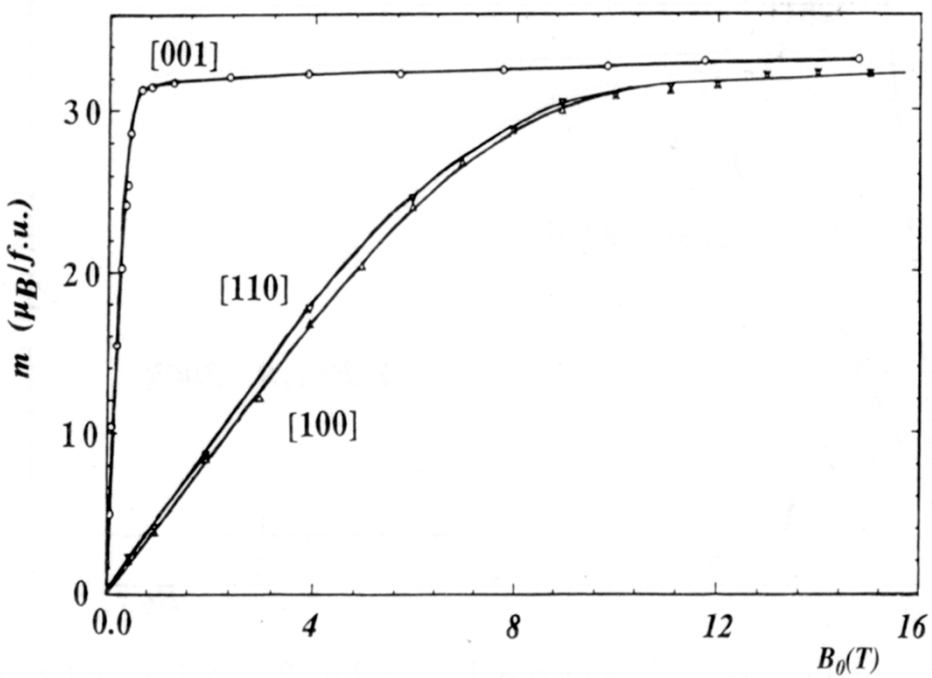

Magnetisation curves for a $Nd_2Fe_{14}B$ single-crystal at room temperature (from *Chikazumi 1997*)

Magnetism in $RE_2Fe_{14}B$

Crystal	M_s at 300K / μ_B/f.u.	H_a at 300K / kOe	T_c / K
$Nd_2Fe_{14}B$	32.5	67	585
$Dy_2Fe_{14}B$	14.0	150	598
$Pr_2Fe_{14}B$	31.9	87	569

Hirosawa *et al.* J. Appl. Phys. 59 (3), 873-879, 1986

Dy couples antiparallel with Fe → lower total moment (ferrimagnetic)

$Nd_2Fe_{14}B$

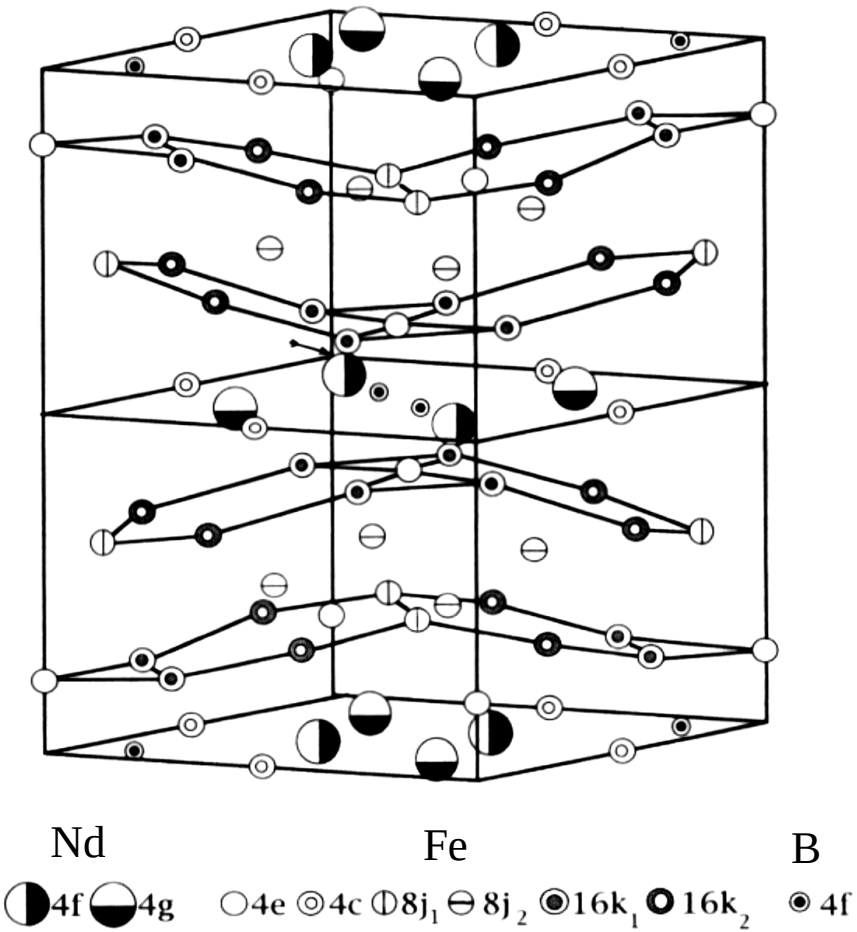

$Nd_2Fe_{14}B$ structure has a tetragonal crystal structure.

It is largely composed of Fe which is abundant and has a large FM moment.

Relatively small amount of abundant light rare earth provide anisotropy.

Tetragonality stabilised by B occupying only 2 vol. %

alternating layers of soft and hard

Magnetic hardening mechanisms

Critical elementary magnetisation reversal processes

- **nucleation magnet ($D >> D_c$)**
  - Nd(Pr)-Fe-B sintered magnet
  - $SmCo_5$ sintered magnet
  - $Sm_2Fe_{17}N_3$
  - hard ferrites
- **pinning magnet ($D >> D_c$)**
  - Sm_2Co_{17} sintered magnet
- **single-domain phenomena ($D \leq D_c$)**
  - rapid quenching
  - mechanical alloying
  - intensive milling
  - HDDR

Initial magnetisation curve

and field dependence of coercivity

in nucleation and pinning-type magnets

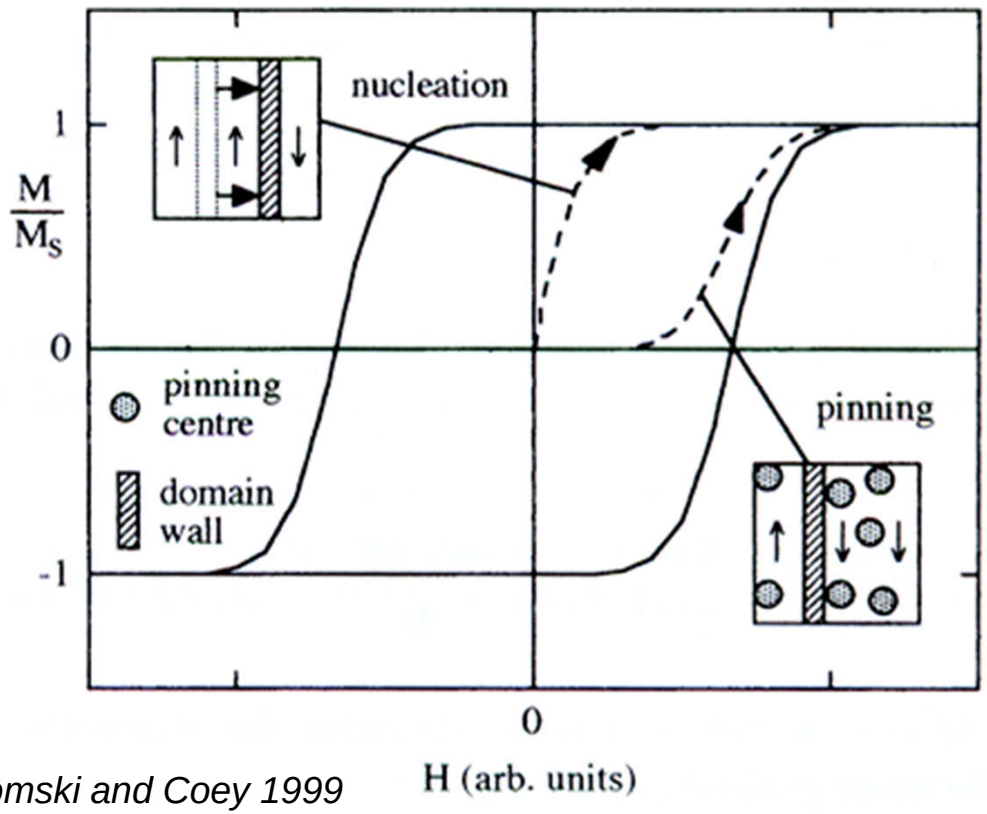

Skomski and Coey 1999

Nd-Fe-B

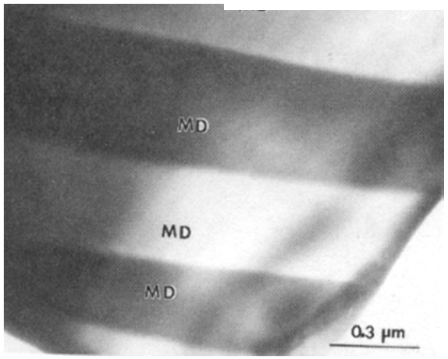

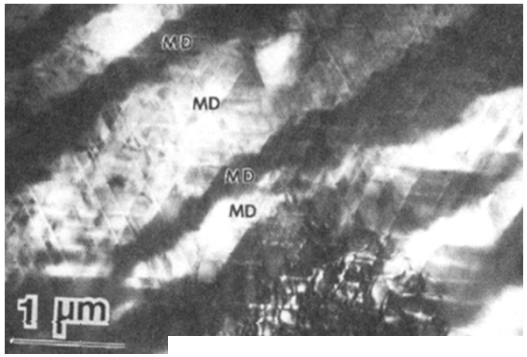

$Sm(CoFeCuZr)_z$

Magnetic structure of permanent magnets

$$E_{\Sigma} = E_{exchange} + E_{anisotropy} + E_{strayfield} + E_{stress} + E_{magnetostrictive} + E_{field}$$

$$E_{\Sigma} \rightarrow \min ; \qquad d_c \sim \sqrt{AK_1}/M_s^2$$

Most relevant are the stray field, exchange and anisotropy energies modifying the domain structure. Even a homogen and continuous sample will show a magnetic domain pattern as it tries to minimise the energy (total) and as the different contributions show non-linear dependencies.

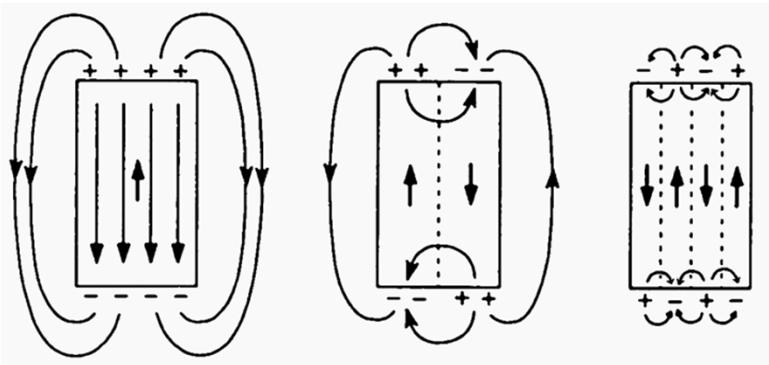

grain size >> single domain size

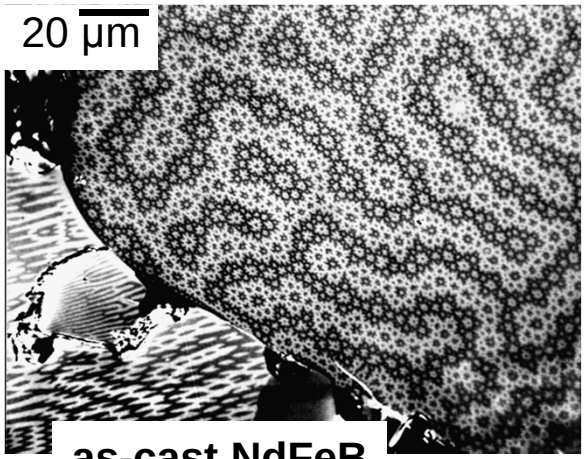

as-cast NdFeB

Size dependence of coercivity

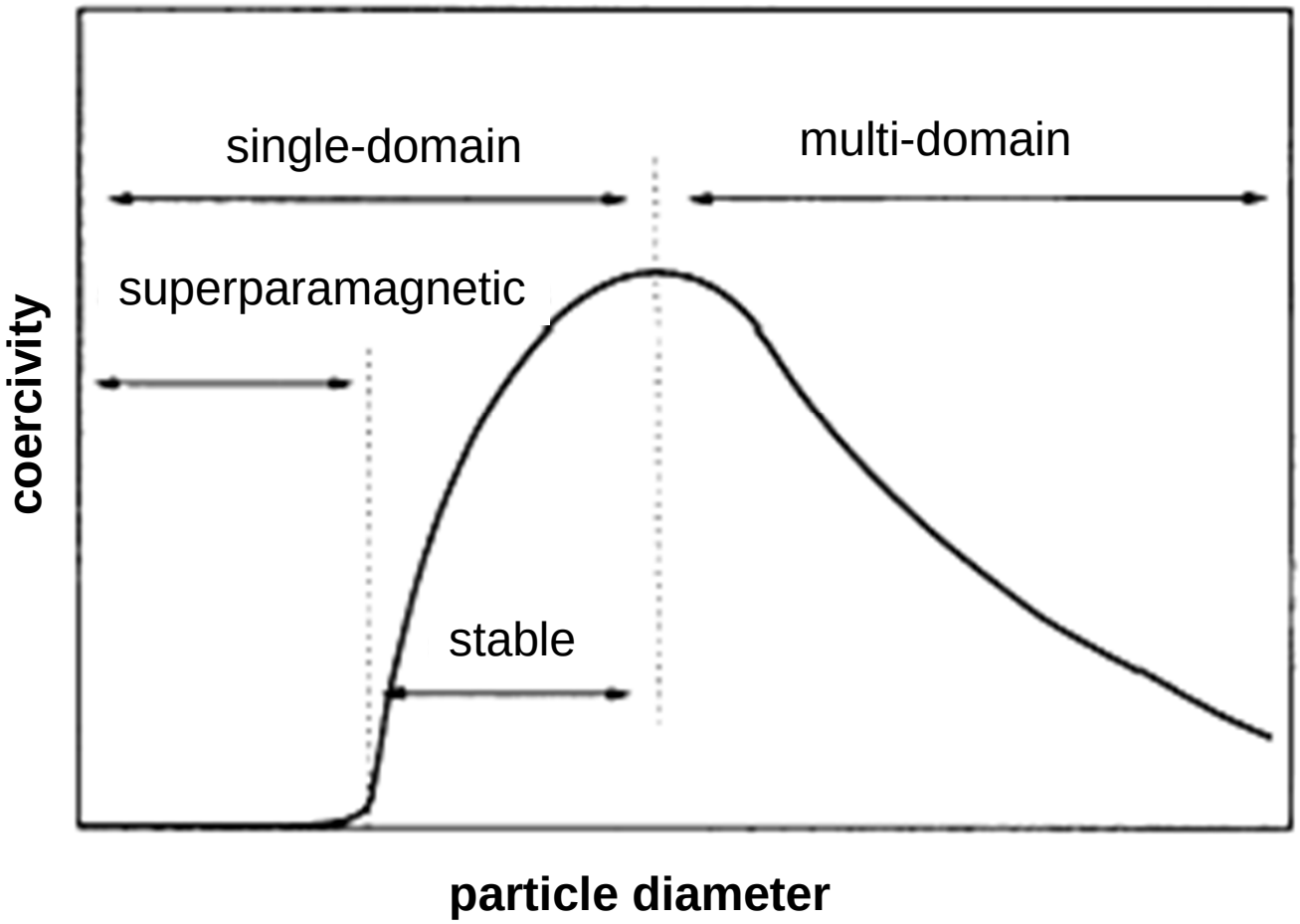

Principle processing routes for PMs

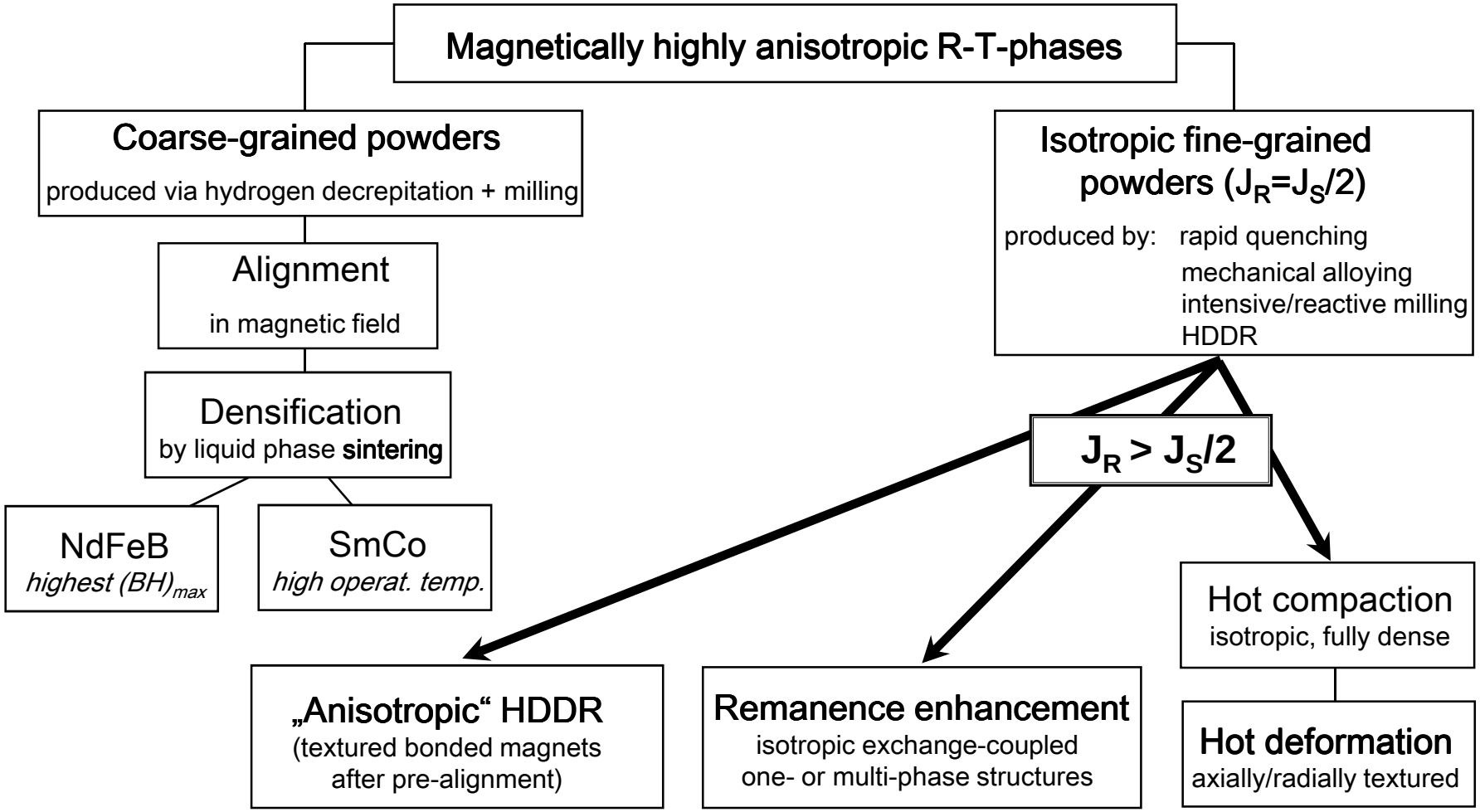

J. Phys. D: Appl. Phys. **33** (2000) R157

NdFeB: Pseudo-Binary Phase Diagram

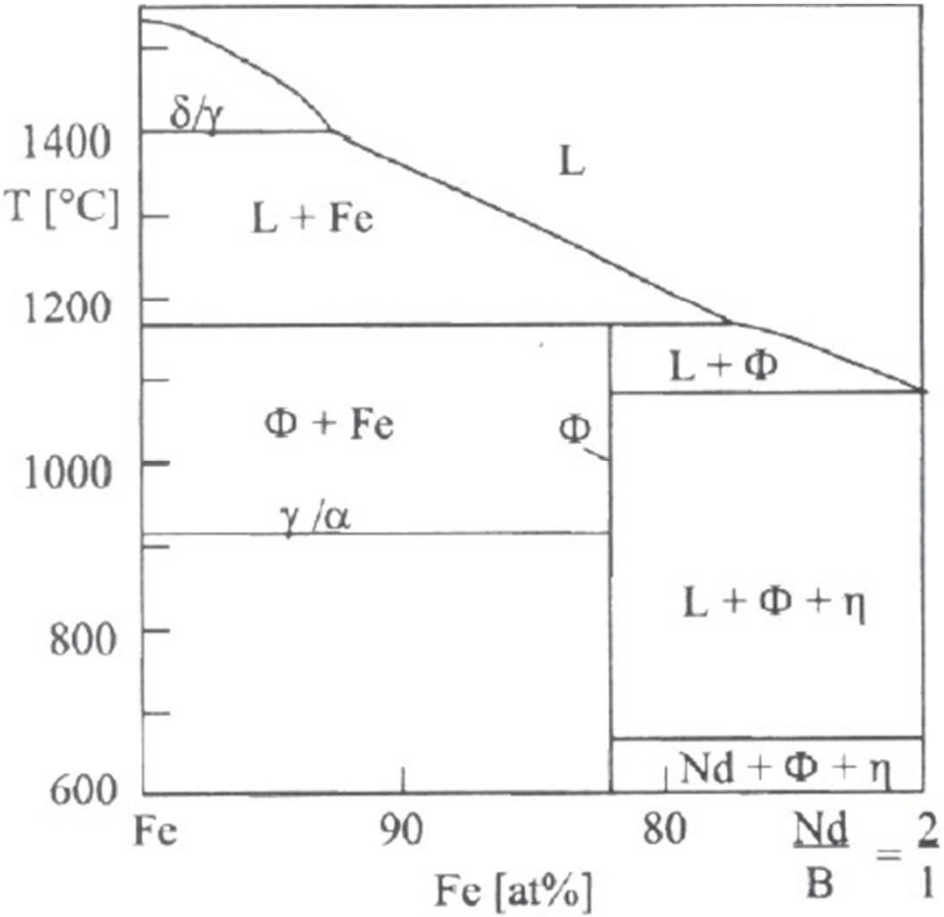

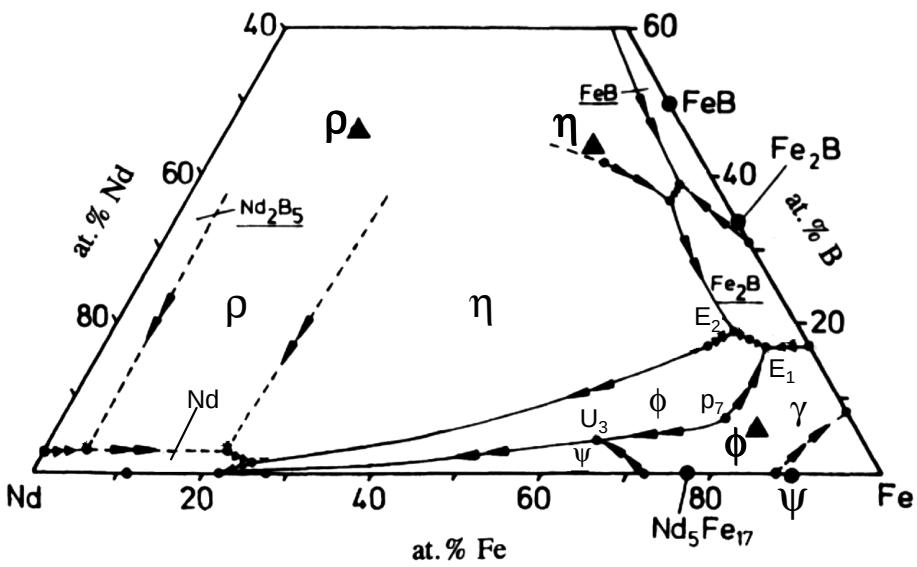

Liquidus projection of the Nd-Fe-B system. Important reactions are p_7 (1180°C: L + g-Fe $\rightarrow$ F), U_3 (1130°C: L + g-Fe $\rightarrow$ F + ψ (Nd_2Fe_{17})), e_4 (1115°C: L $\rightarrow$ η + F), E_1 (1105°C: L $\rightarrow$ F + + g-Fe + Fe_2B) and E_2 (1095°C: L $\rightarrow$ η + F + Fe_2B), (after *Knoch et al. 1994*).

Processing

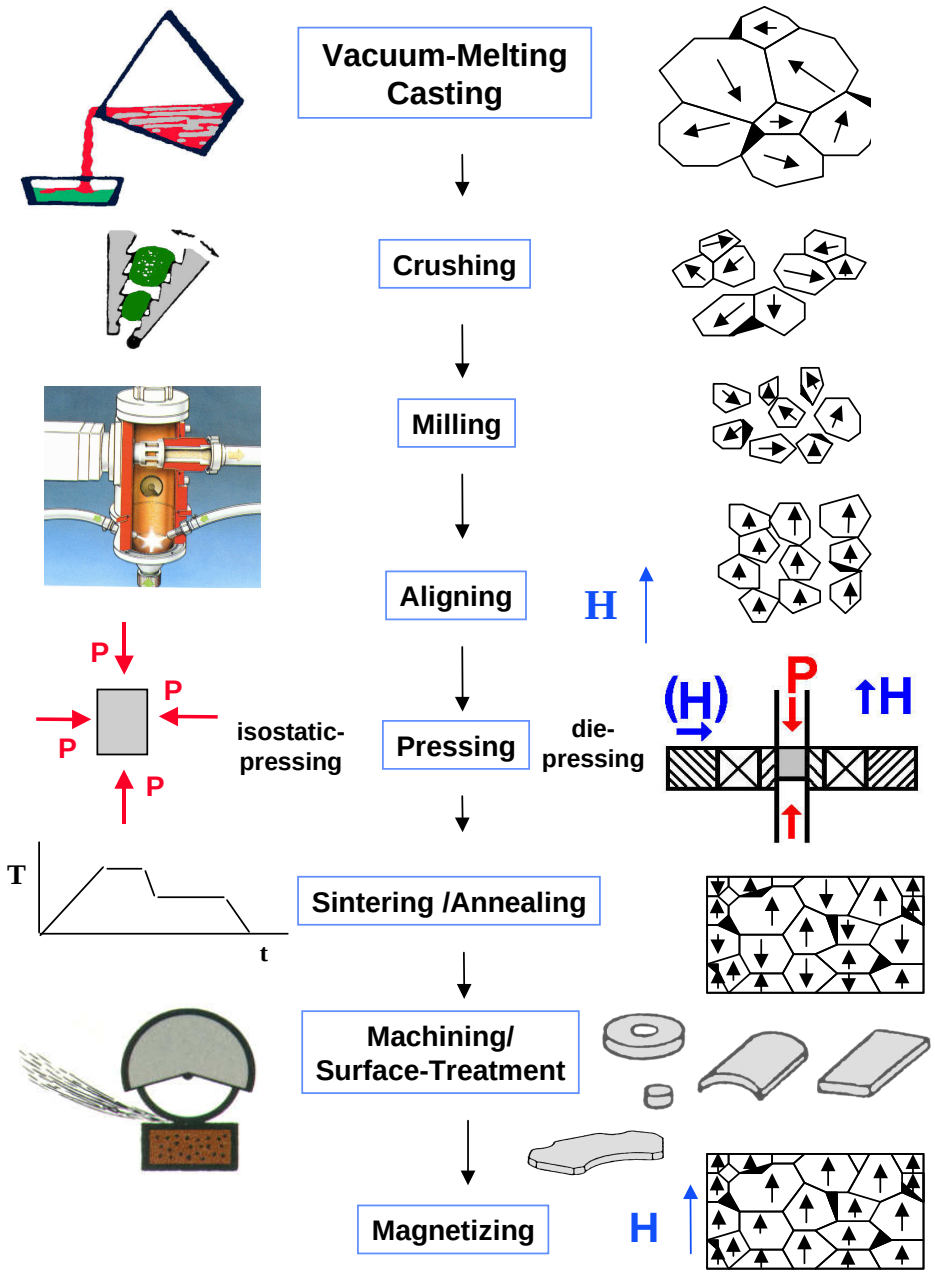

Courtesy:
Vacuumschmelze GmbH

Hydrogen Decrepitation (HD)

Video

[redacted]

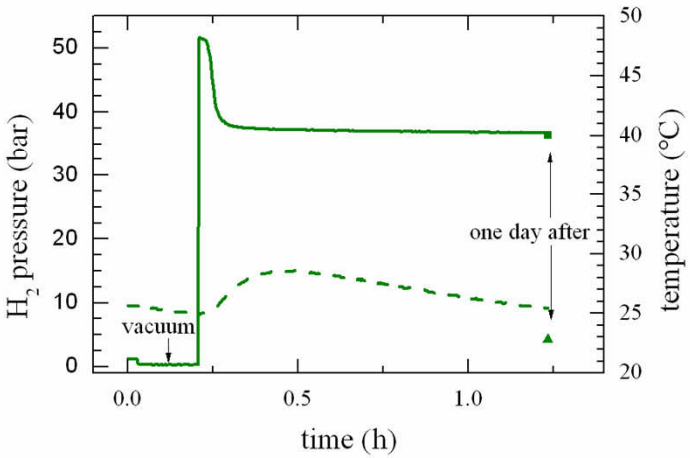

NdFeB sintered magnet manufacturing

Ningbo Tongchuang Strong Magnet Material Co., Ltd

NdFeB sintered magnet manufacturing

Ningbo Tongchuang Strong Magnet Material Co., Ltd

Textured NdFeB sintered magnets

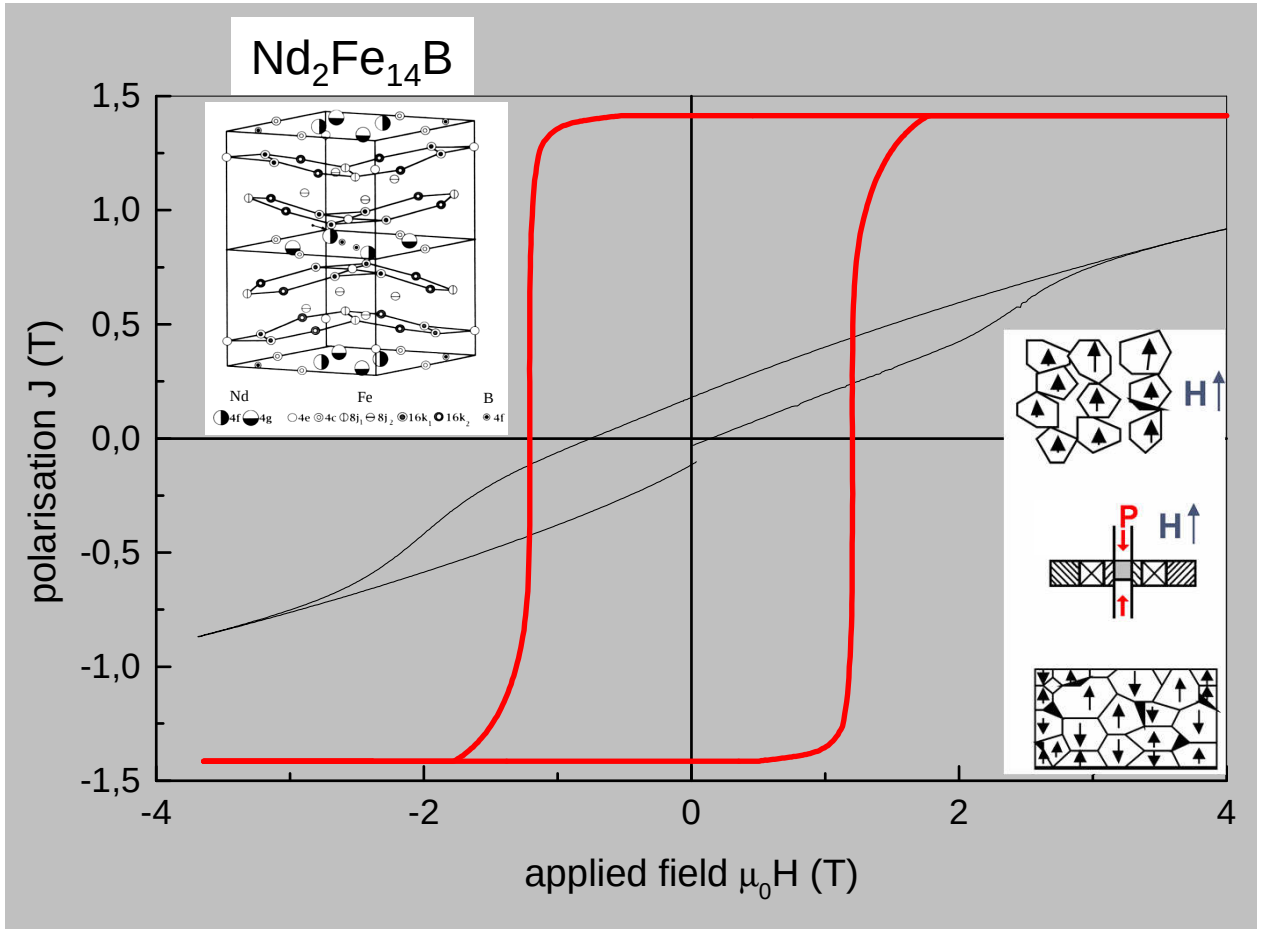

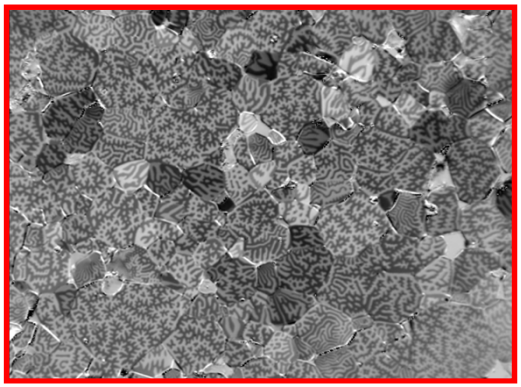

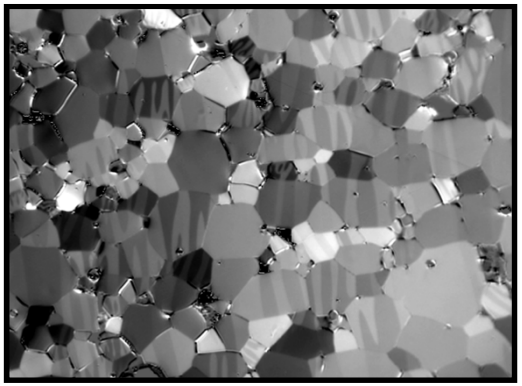

5µm

macrotexture ↔ microtexture

magnetic measurements ↔ Kerr microscopy

Multiscale characterisation I

effect of Nd-rich phase at the grain boundaries

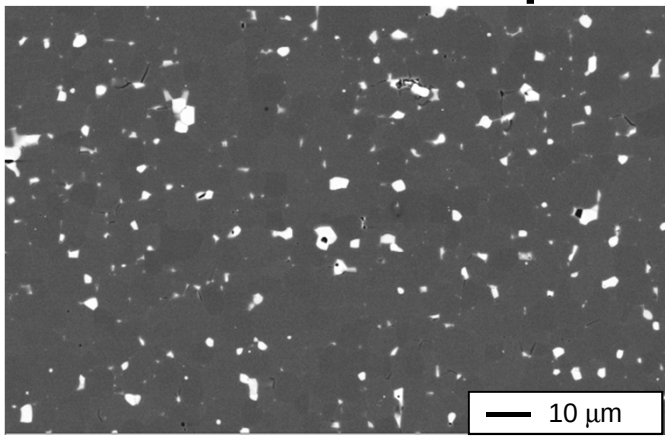

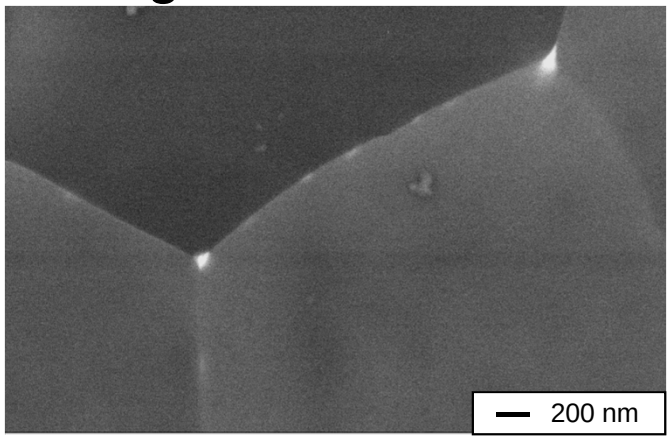

correlation of EBSD with magnetic domain structure

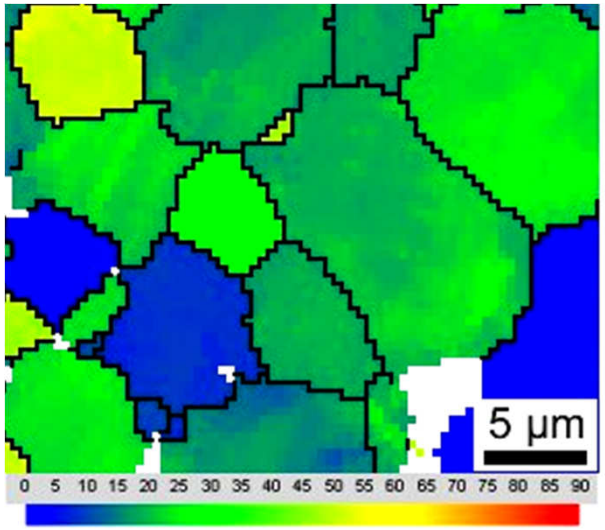

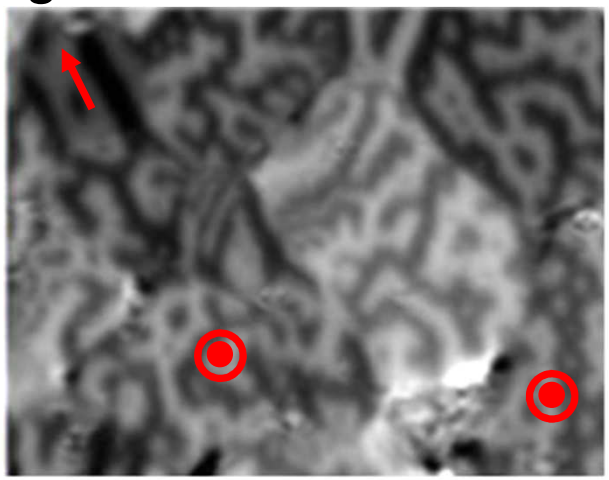

Multiscale characterisation

$Nd_2Fe_{14}B$ | Nd_2O_3 | NdO and fcc Nd-rich

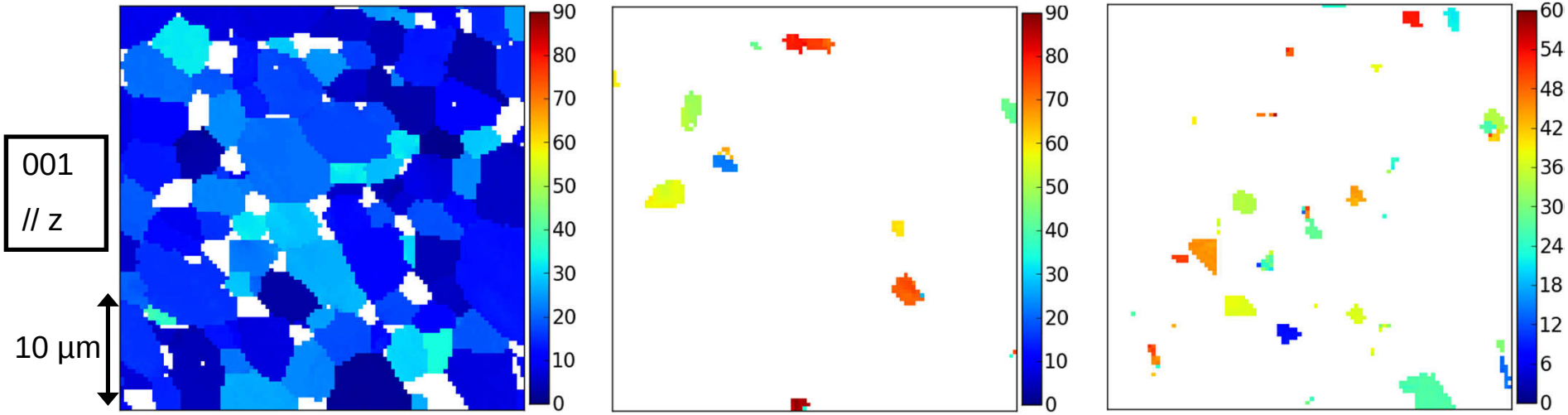

Acta Mat. 59 (2011) 1026

Phase map

Nd_2O_3

fcc

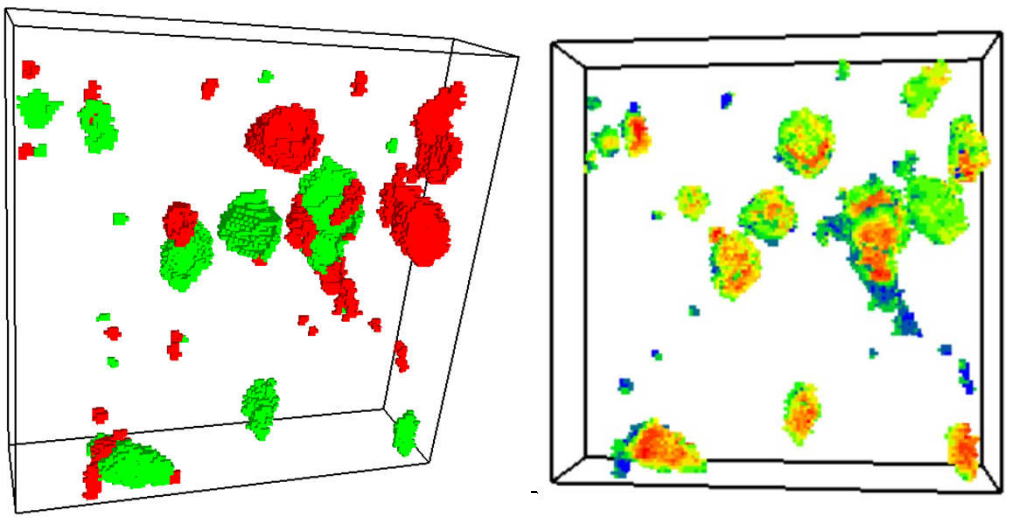

3D-EBSD and EDX

O map

Oxides exist 8 µm below surface
→ not preparation artefacts

TECHNISCHE UNIVERSITÄT DARMSTADT

Multiscale characterisation II

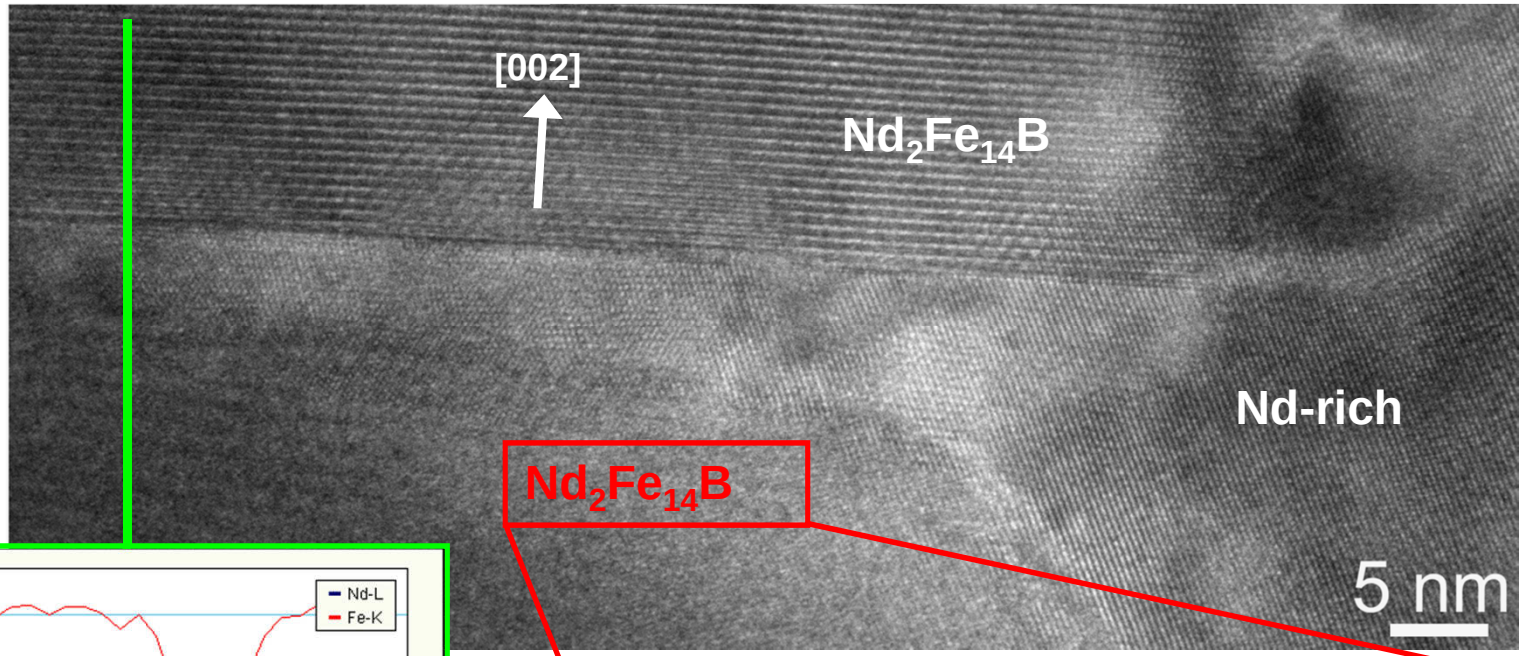

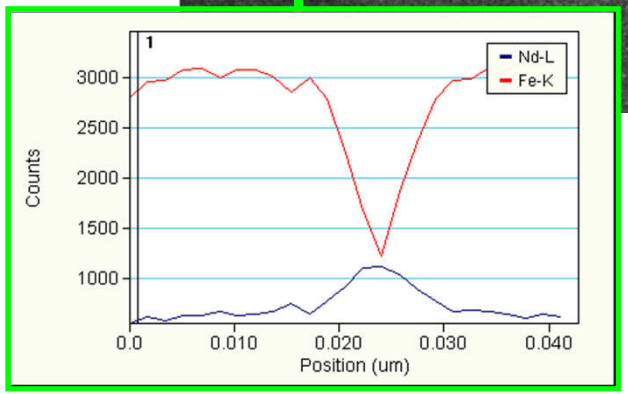

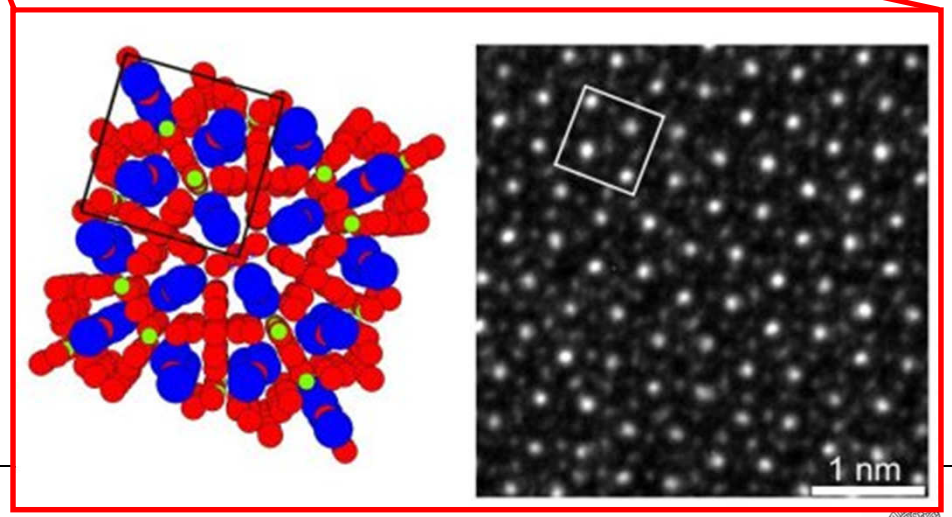

EDX line-scan across gb phase

T.G. Woodcock et al, IFW Dresden

Atomistic calculations of local magnetic anisotropy

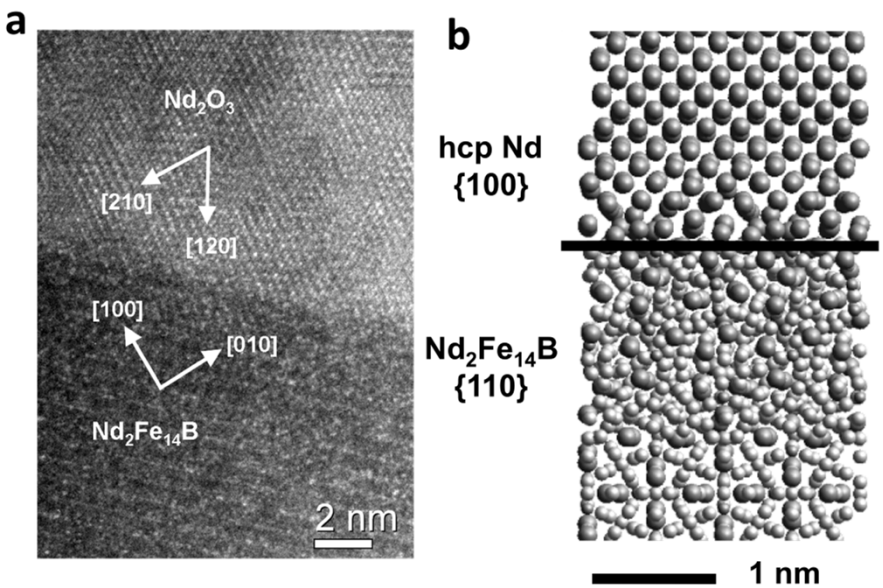

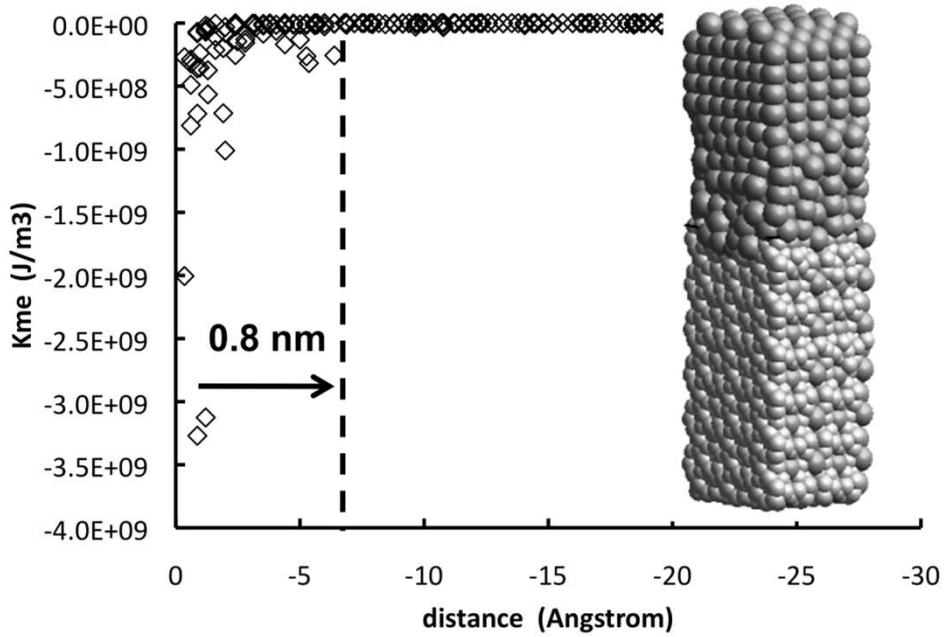

(a) HRTEM shows interface area between a $Nd_2Fe_{14}B$ grain and a Nd-rich phase.

(b) Calculated boundary of an equivalent grain boundary configuration.
Top layer: hcp Nd {100} surface facing the grain boundary. Bottom: NdFeB {110} surface facing the grain boundary.

Magnetoelastic anisotropy as function of distance for $Nd_2Fe_{14}B$ (100) surface cut, c-axis parallel to interface to a fcc Nd (011) surface, the plane orientation is in respect to the interface.
Inset: Top layer is the fcc Nd rich phase, bottom layer is the $Nd_2Fe_{14}B$ phase.

APL, cooperation with G. Hrkac / T. Schrefl (Uni Exeter/ St. Pölten)

Scripta Mat. ***67*** *(2012) 536*

Advanced nanostructured hard magnets

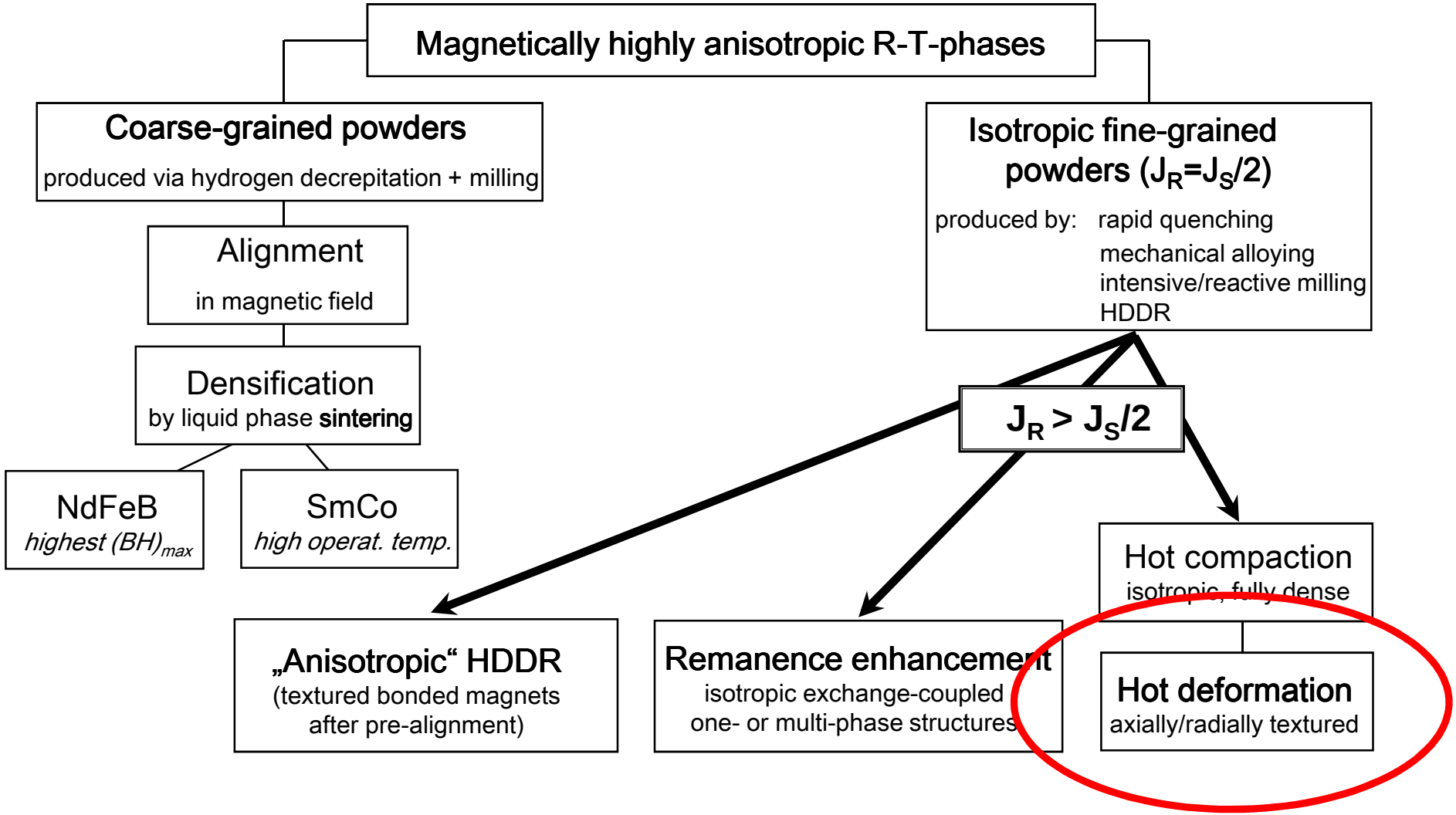

Textured magnets by hot deformation

Texture in fine grained NdFeB magnets

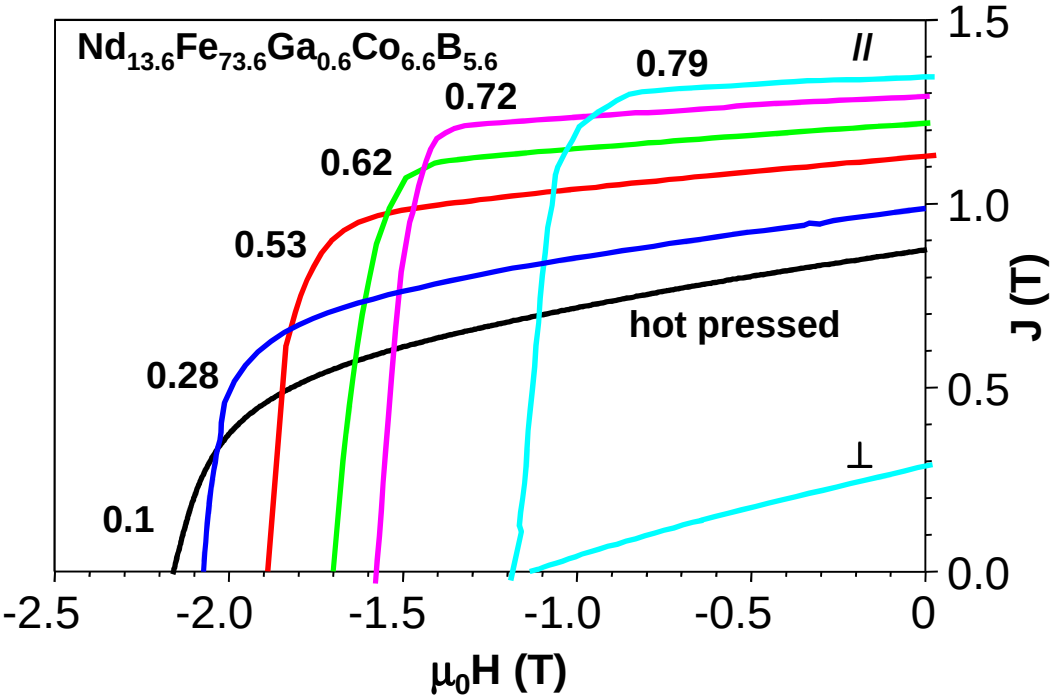

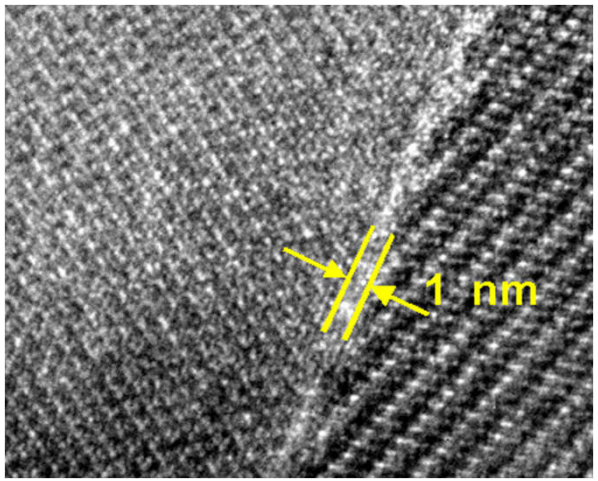

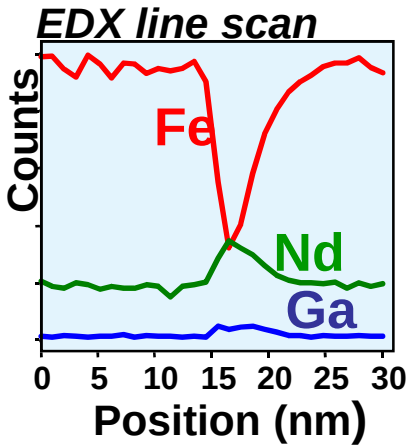

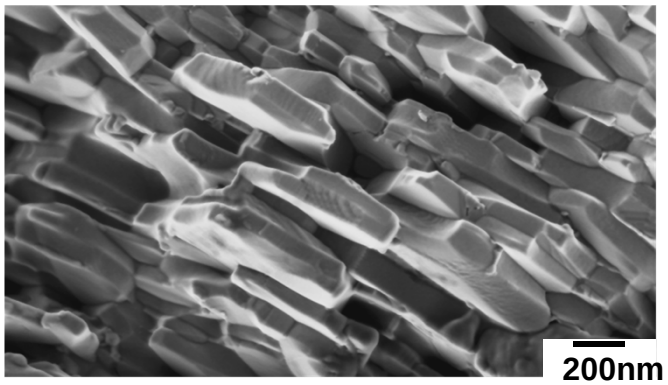

Texture in fine grained NdFeB magnets

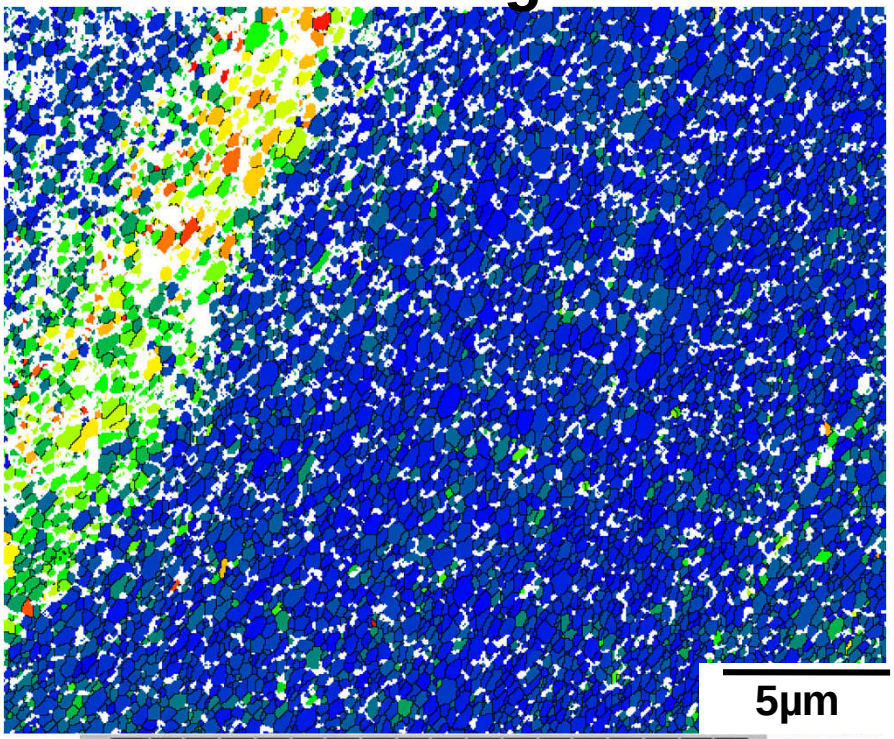

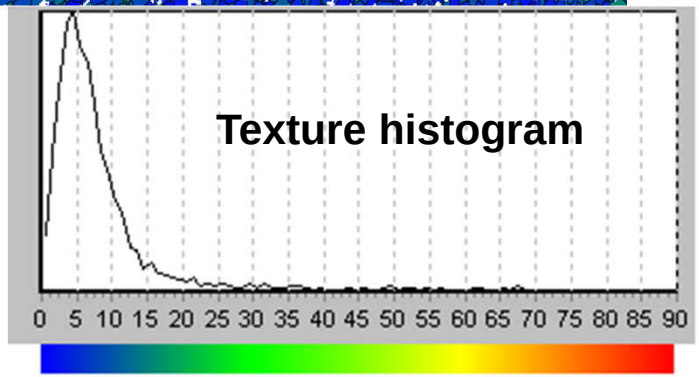

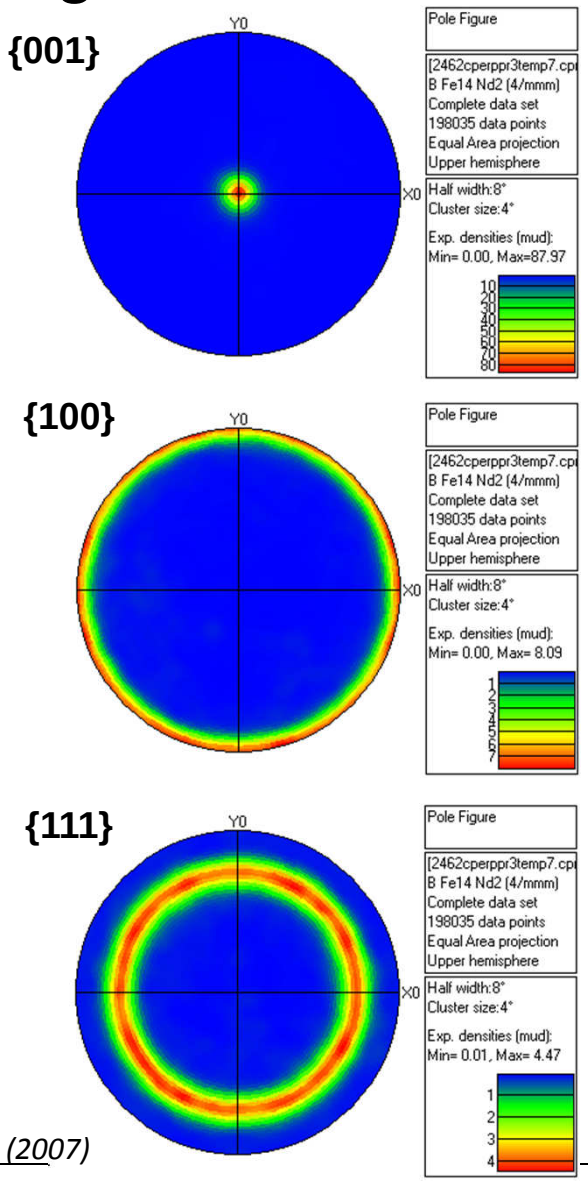

K. Khlopkov, O. Gutfleisch, D. Hinz, K.-H. Müller, L. Schultz, J. Appl. Phys. 102, 023912 (2007)

Interaction domains

Imants Dirba and Simon Sawatzki, TU Darmstadt

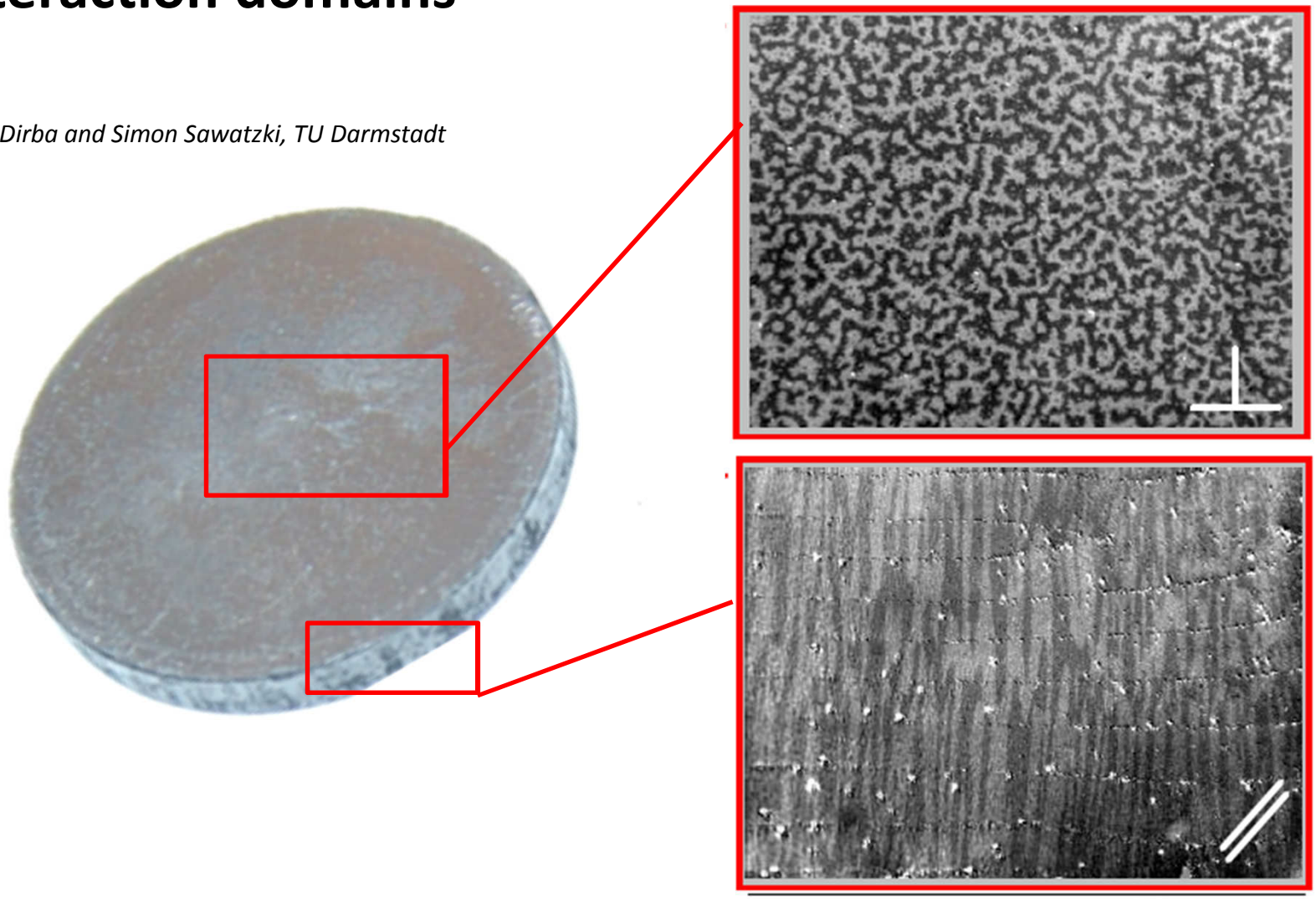

K. Khlopkov, O. Gutfleisch, D. Hinz, K.-H. Müller, L. Schultz, J. Appl. Phys. 102, 023912 (2007)

Interaction domains

in die-upset magnets consisting of only melt-spun NdFeB ribbons

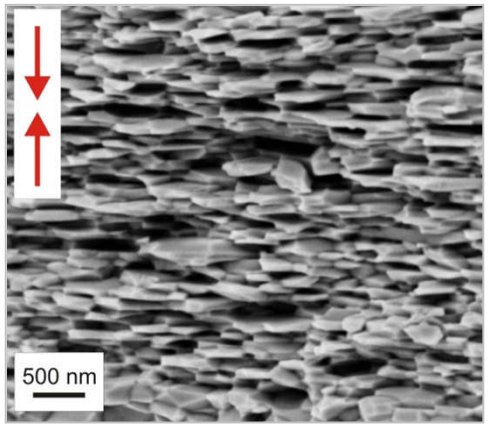

fractured surface:
plate-like grains with thickness of 100…200 nm and lateral expansion of 400…500 nm

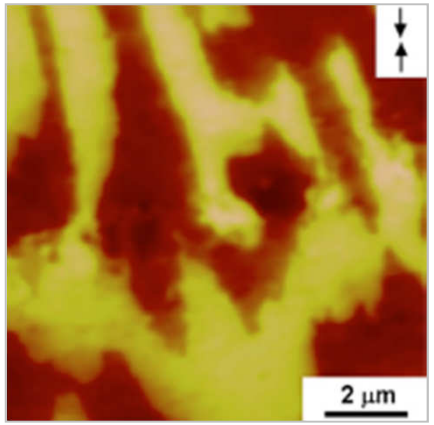

MFM picture of interaction domains in die-upset NdFeB magnet

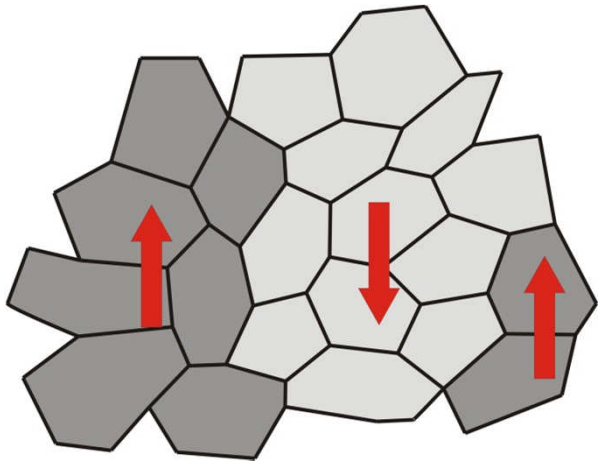

interaction domains encompass several grains

D. J. Craik and E. D. Isaac, Proc. Phys. Soc. 76, 160 (1960)

L. Folks, R. Street, R.C. Woodward, Appl. Phys. Lett. 65 (7), (1994)

K. Khlopkov, O. Gutfleisch, D. Hinz, K.-H. Müller, L. Schultz, J. Appl. Phys. 102, 023912 (2007)

Cooperative phenomena in fine grained NdFeB

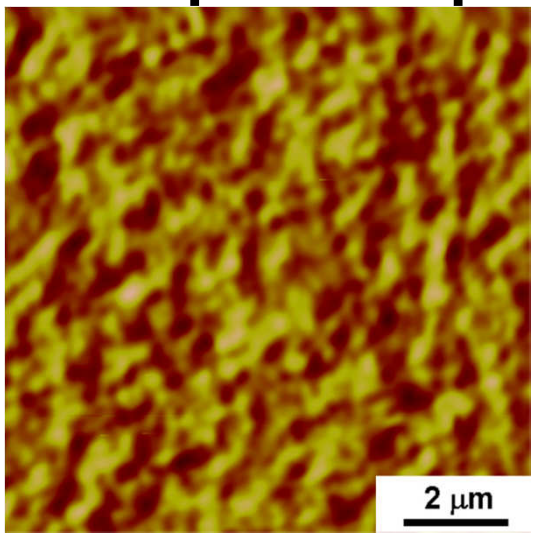

0.1

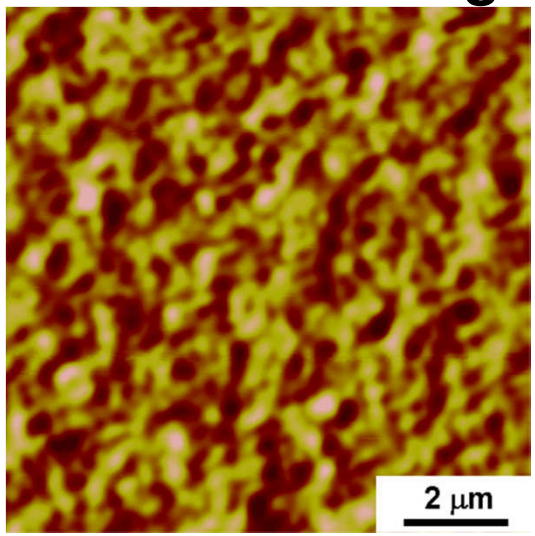

0.28

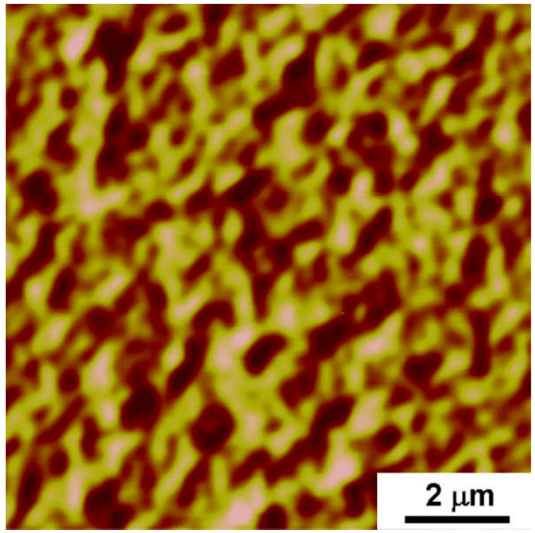

0.53

$(B_r^{\parallel}-B_r^{\perp})/B_r^{\parallel}$

0.62

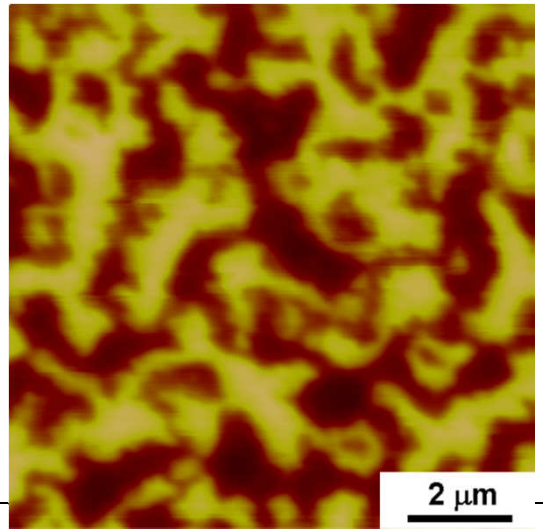

0.72

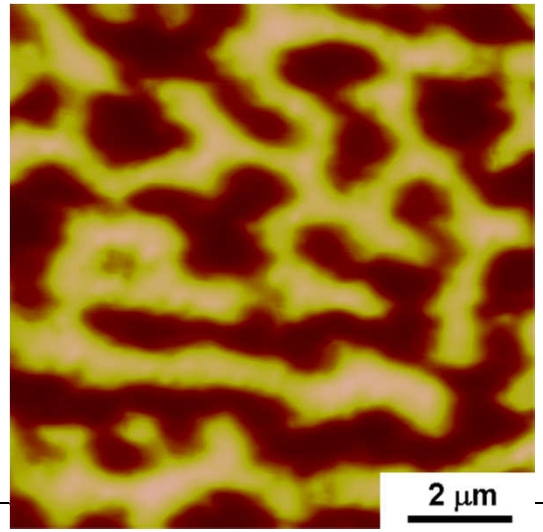

0.79

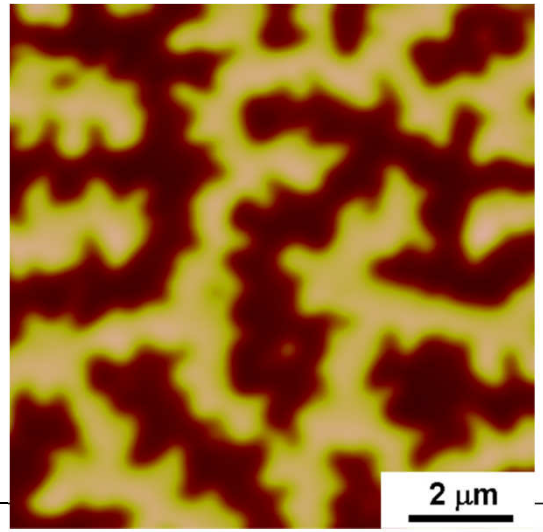

Conventional and superconducting permanent magnets

Stable position of heavy objects in midair (> 1kg / cm^2)

Levitation

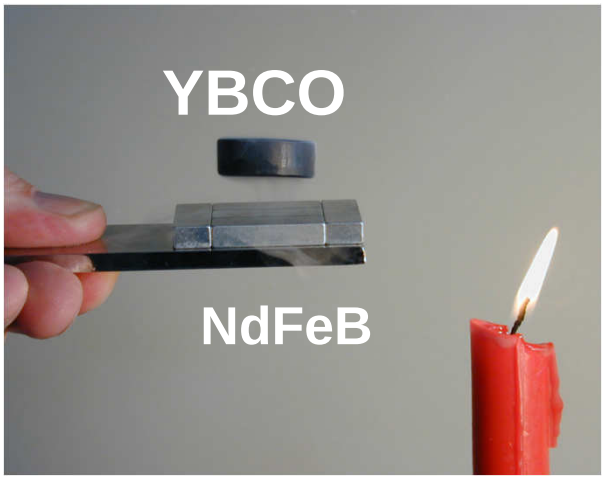

Suspension

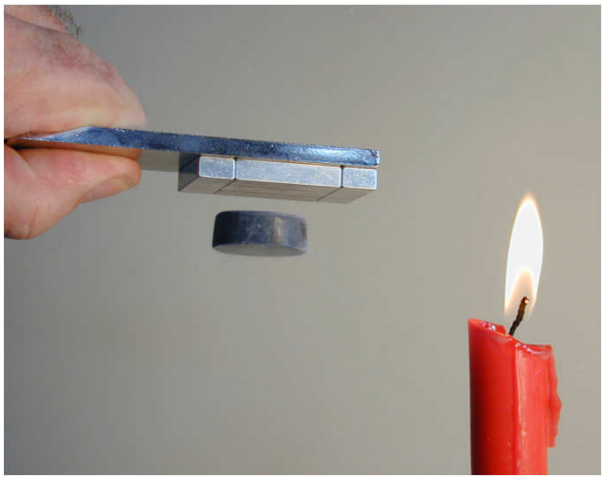

Cross stiffness

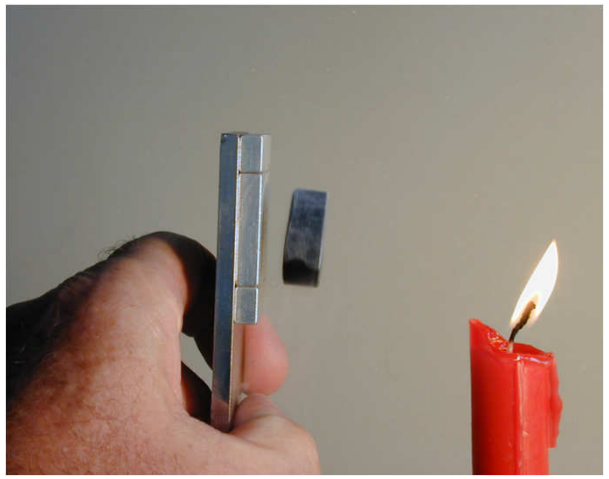

- by varying the spatial distribution of the external field, the position of the superconducting magnet may have different degrees of freedom :

0 D – as in the examples above
1 D – as a train on a rail
2 D – for fields being homogeneous in x, y directions

- the same holds for rotational degrees of freedom

⇒ flywheels, bearings and transport systems

Superconducting bearing

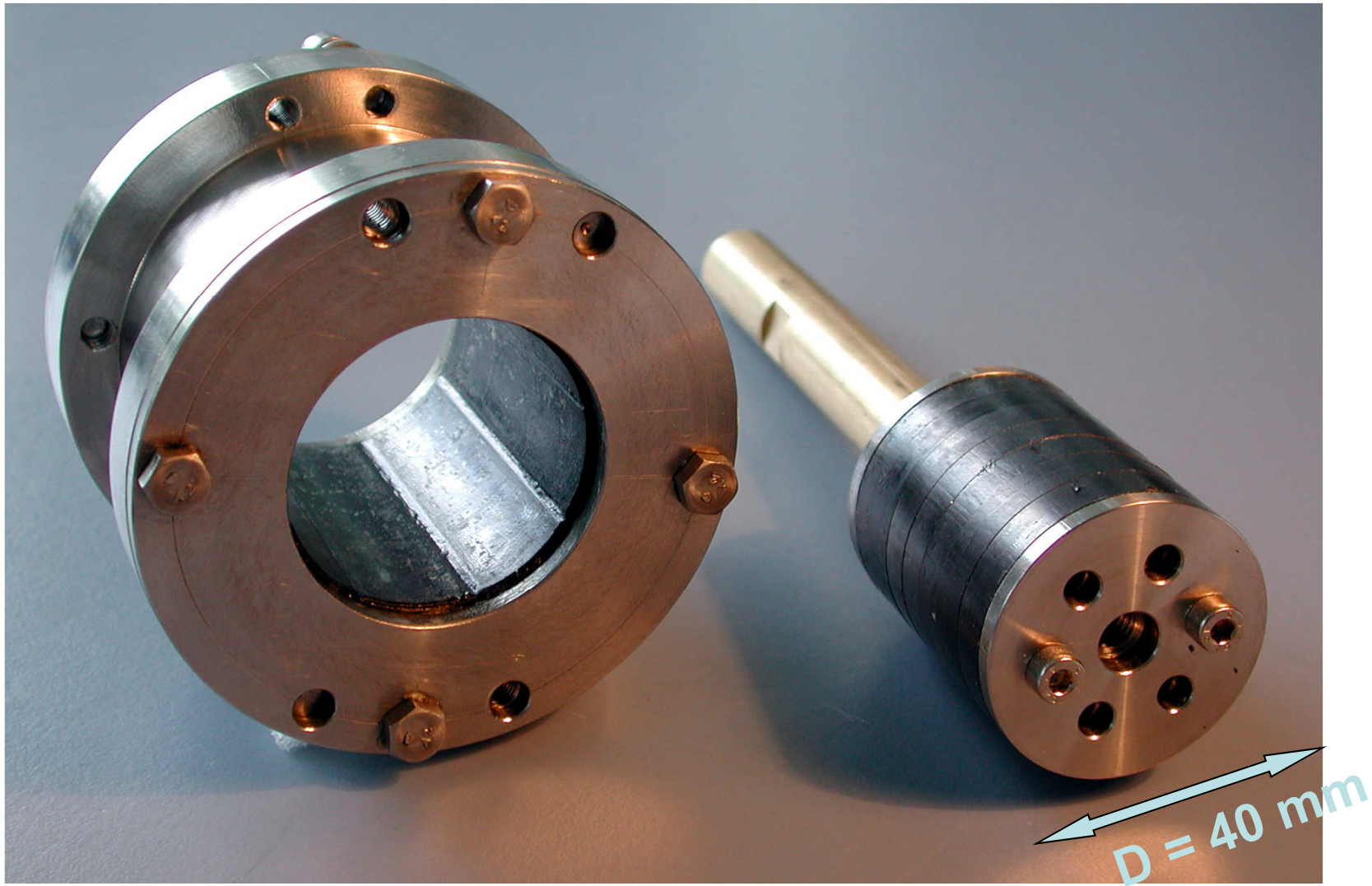

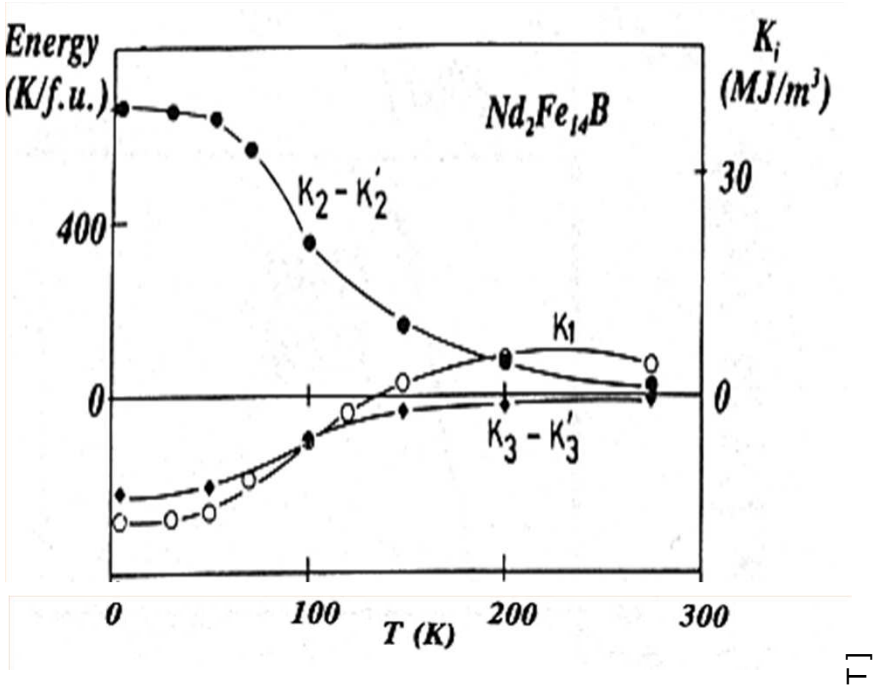

Anisotropy constants of
$Nd_2Fe_{14}B$
in dependence on temperature

spin reorientation in $Nd_2Fe_{14}B$ for T < 135 K

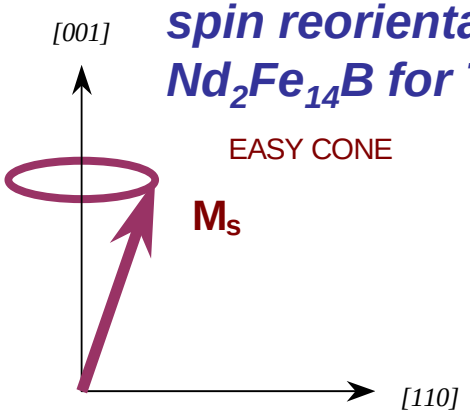

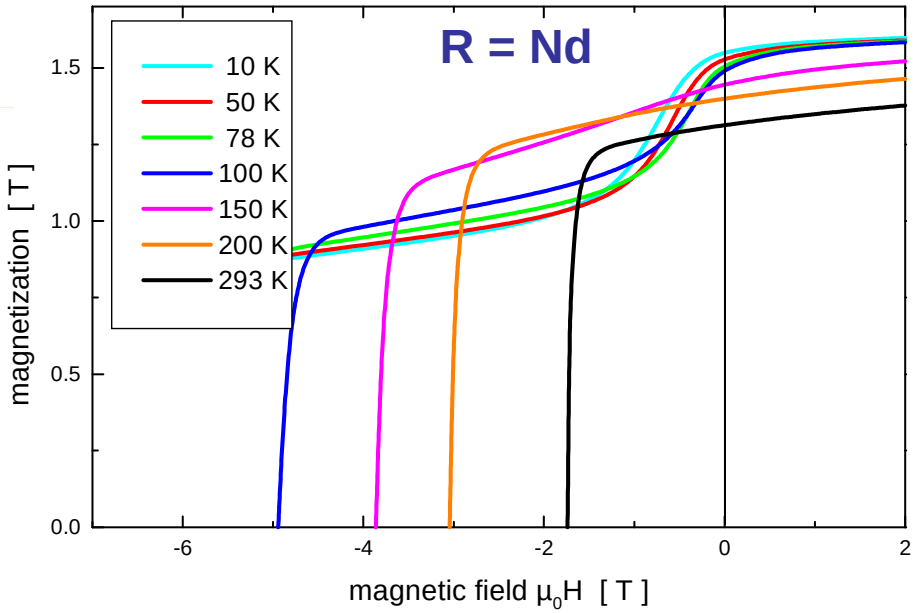

Compound	T_C (K)	$\mu_0 H_A$ (T)	K_1 (MJm^{-3})	$\mu_0 M_S$ (T)	$(BH)_{max}$ (kJm^{-3})	δ_w (nm)	d_c (nm)
$Nd_2Fe_{14}B$	585	6.7	4.9	1.60	516	4.2	300
$Pr_2Fe_{14}B$	565	8.7	5	1.56	484	~ 4	~300

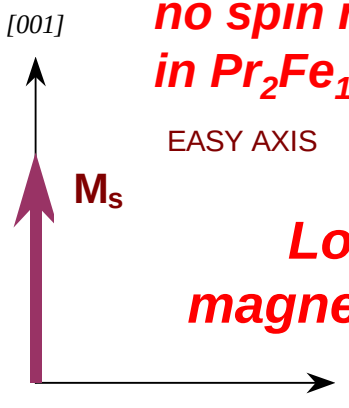

no spin reorientation in $Pr_2Fe_{14}B$

EASY AXIS

Low temperature magnets for SC bearings

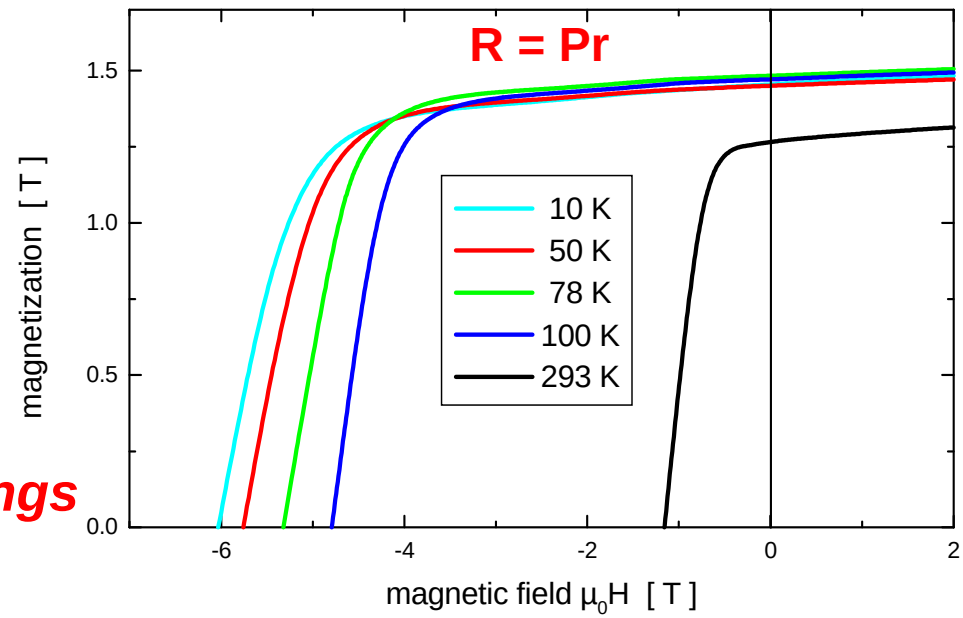

TECHNISCHE UNIVERSITÄT DARMSTADT

Sm-Co phase diagram

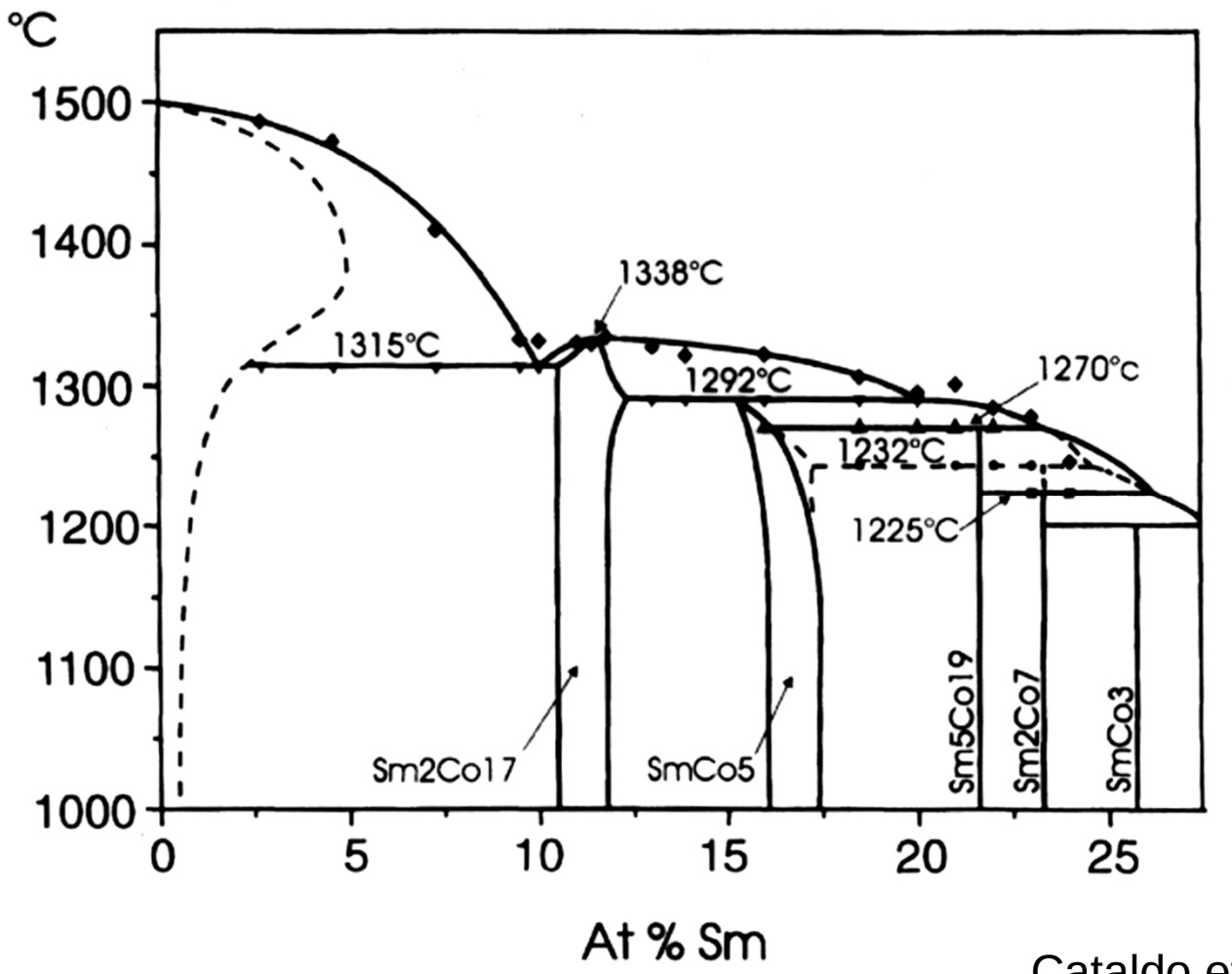

Cataldo et al., 1996

STRUCTURAL TRANSFORMATION in the 2:17 SmCo SYSTEM

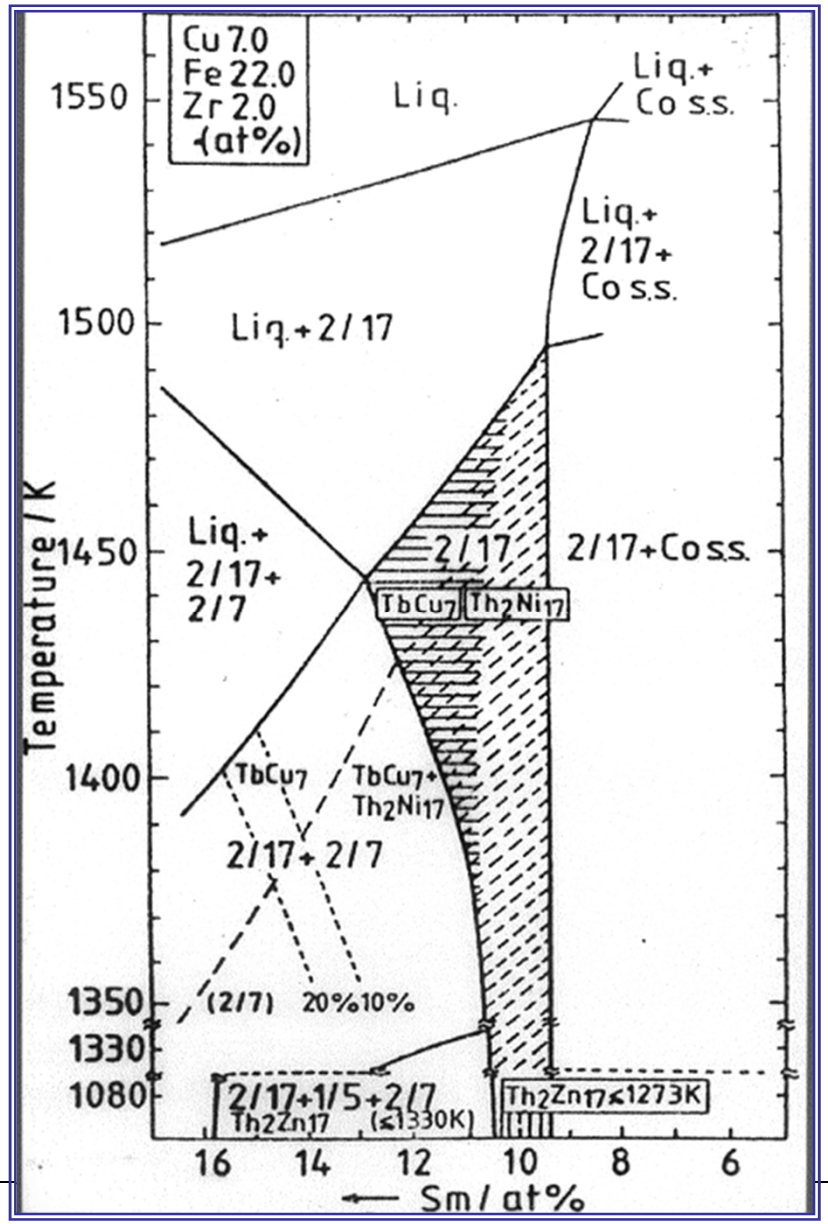

HEAT-TREATMENT	STRUCTURE
Sintering (1210-1230^{0}C)	•2:17 H formation •Elements taken into solution •Densification
Solution treatment (1180 –1200^{0}C)	•1:7 H formation •Fe atoms occupy planar sites
Quenching to RT	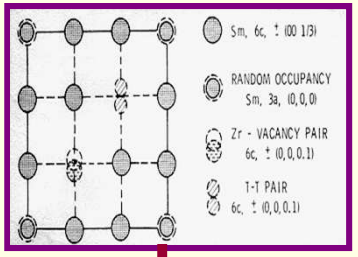
Isothermal aging (800 – 875^{0}C) & Slow cooling to 400^{0}C @ 0.5 – 1.0^{0}C/ min	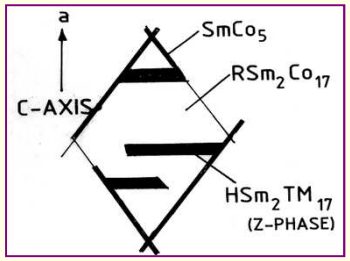

TECHNISCHE UNIVERSITÄT DARMSTADT

Precipitation hardening

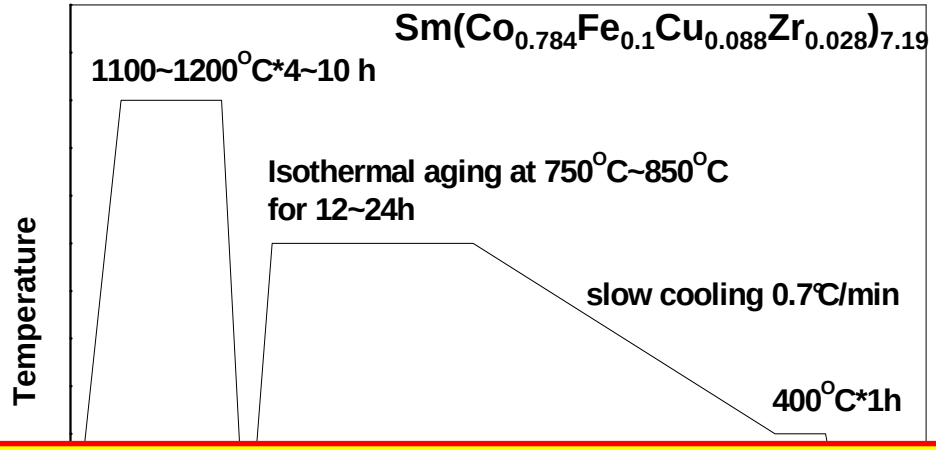

Morphology of Sm_2Co_{17} - magnets with their characteristic structural length scales in the *nm* range is independent of the processing procedure

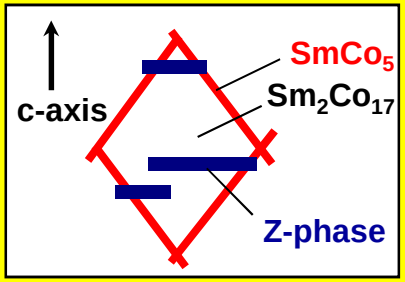

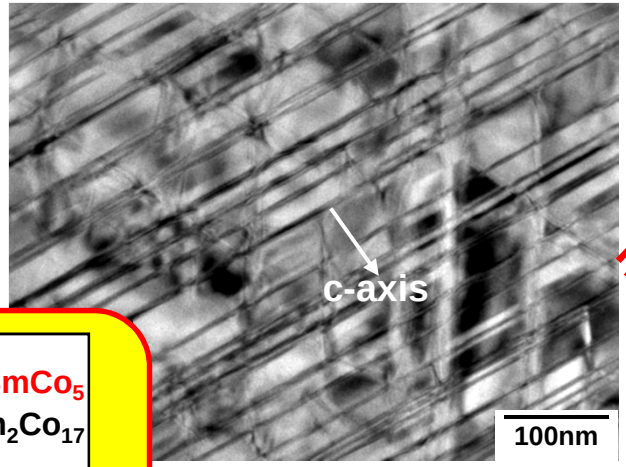

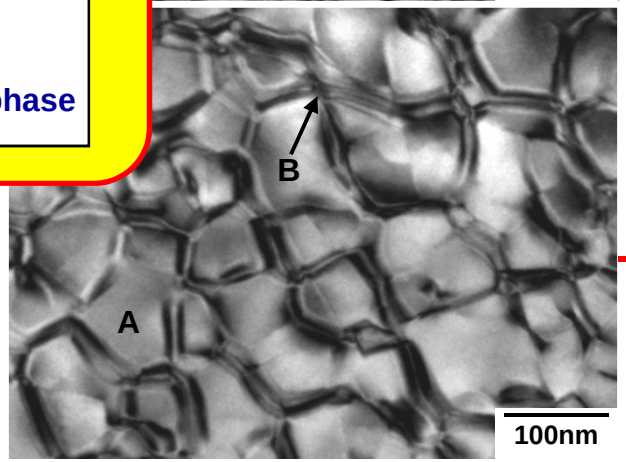

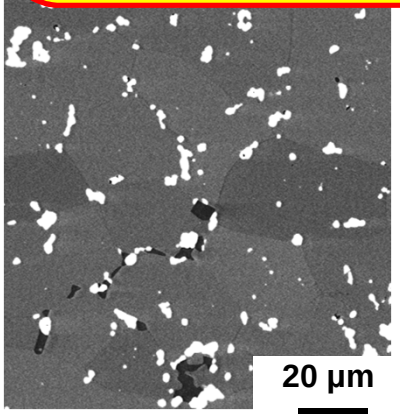

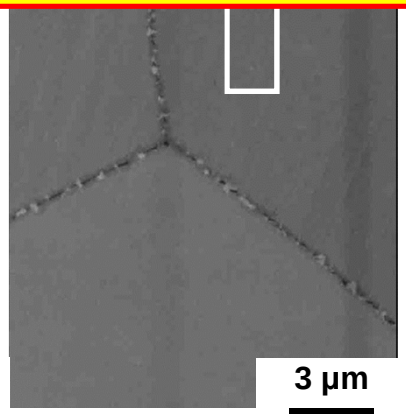

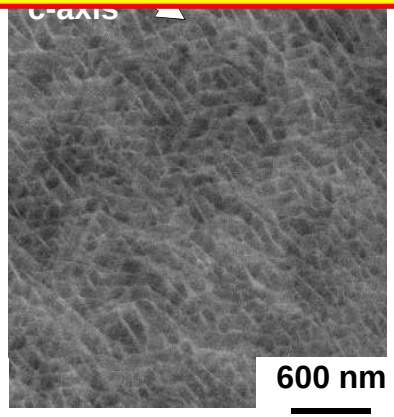

Schematic $H_a(T)$ dependence leading to different pinning modes

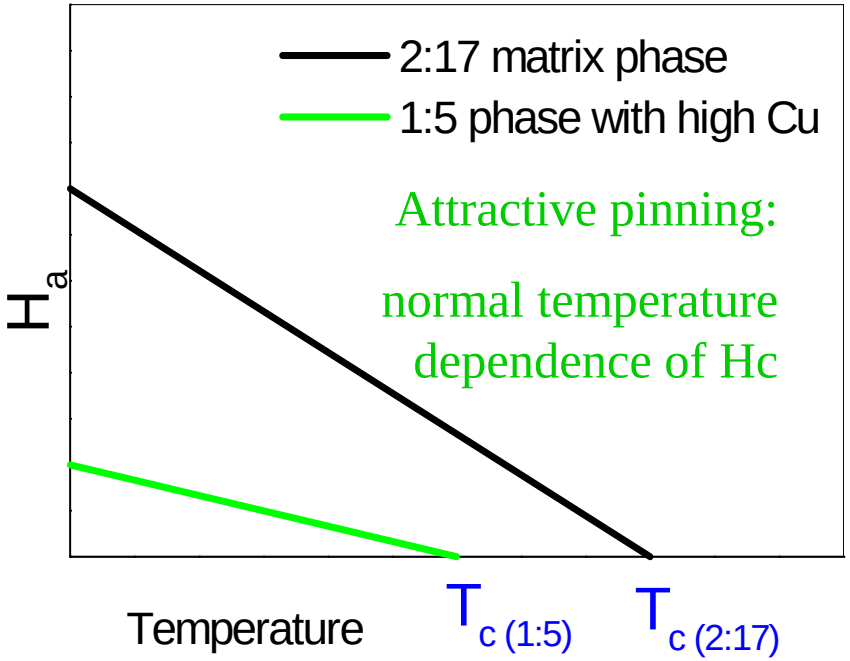

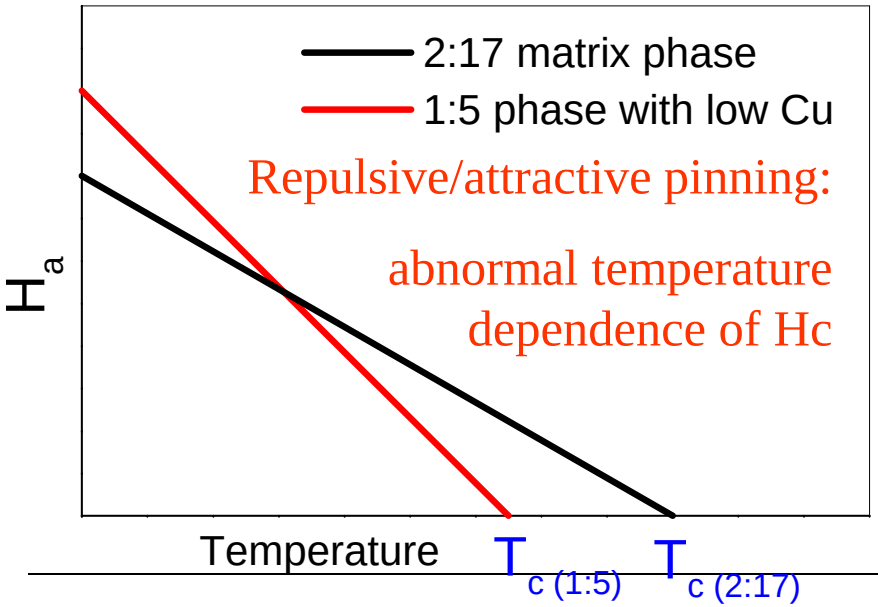

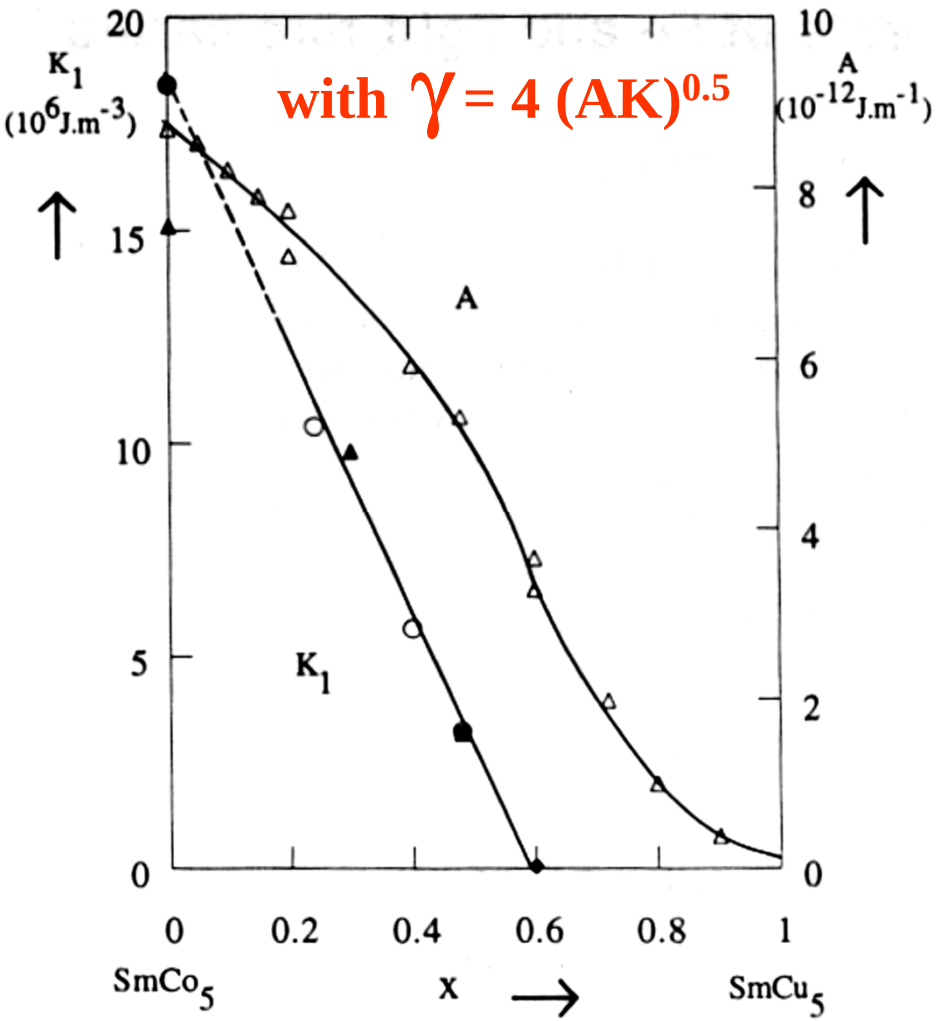

Lectard et al, J. Appl. Phys. 75 (1994) 6277

Advanced nanostructured hard magnets

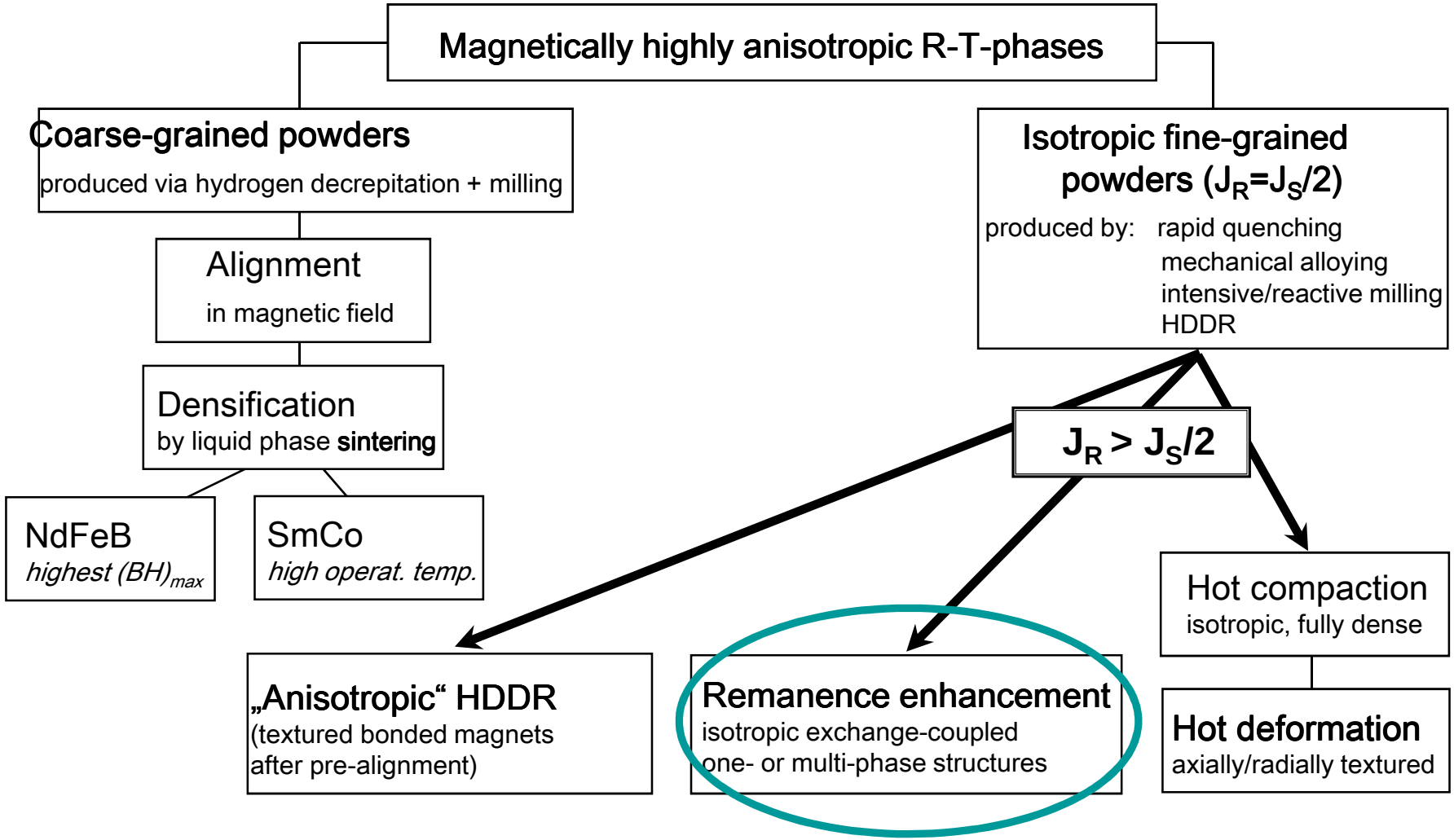

Isotropic remanence-enhanced magnets

Prototypes of RPM's based on $R_2Fe_{14}B$ with idealised microstructures

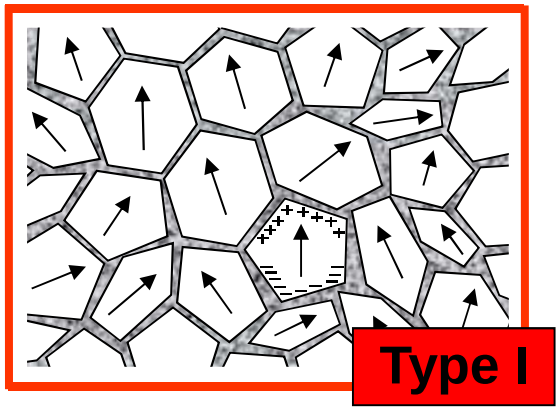

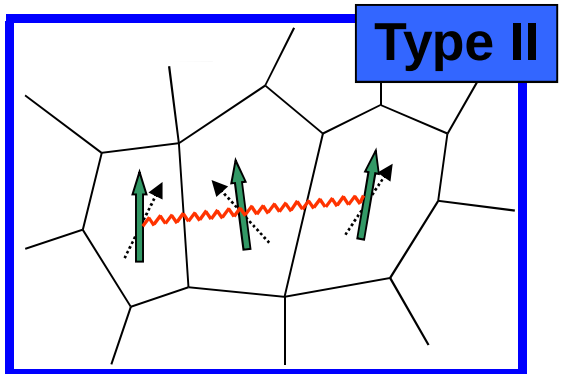

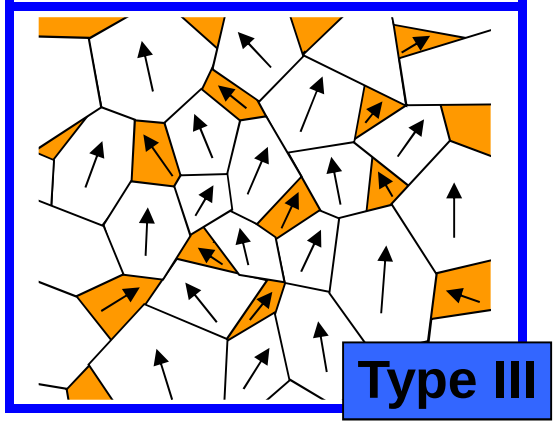

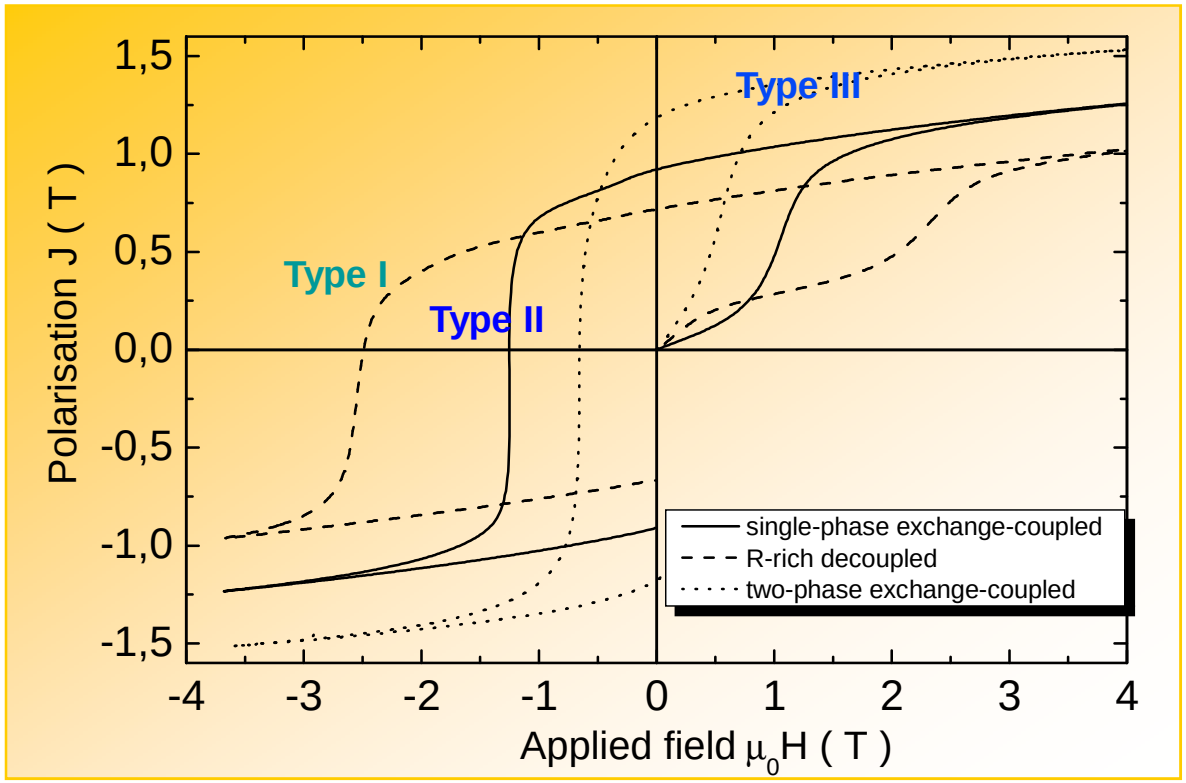

Type I: decoupled grains separated by thin paramagnetic layer → ↑ H_c

Type II: exchanged coupled grains based on stoichiometric $R_2Fe_{14}B$

Type III: exchanged coupled grains based on nanocomposite $R_2Fe_{14}B$ / α-Fe (exchange-spring mechanism)

→ ↑ J_r

Remanence enhancement: $M_r/M_s > 0.5$

- **single-phase exchange coupled magnets**

  McCallum, Clemente et al. (1987, 1988)

  Hadjipanayis et al. (1988)

  Schultz et al. (1988)

  Davies et al. (1991)

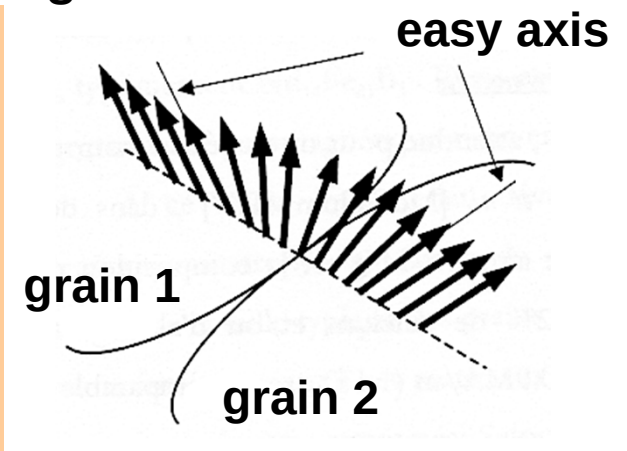

exchange-spring behaviour
large recoil-permeability

- **nanocomposite magnets**

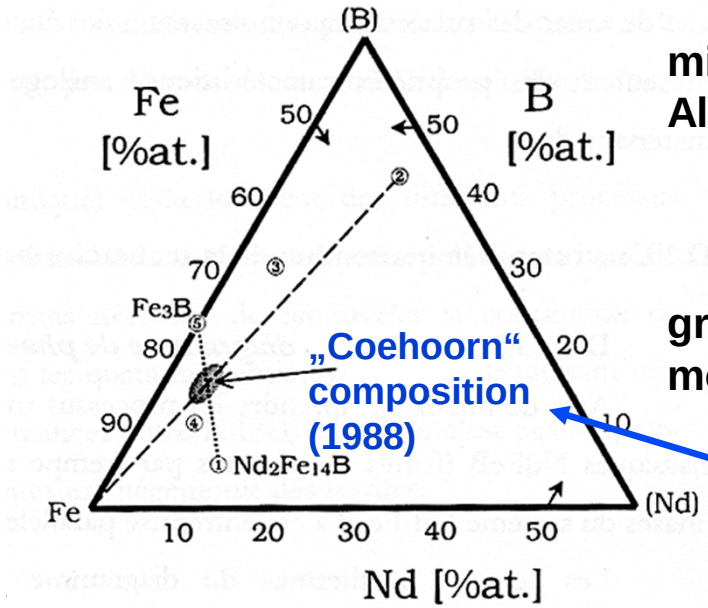

microalloying:
Al, Si, V, Cr, Cu, Nb, Ga

optimisation

grain refinement and modifications of tie-lines

$Nd_4Fe_{78}B_{18}$

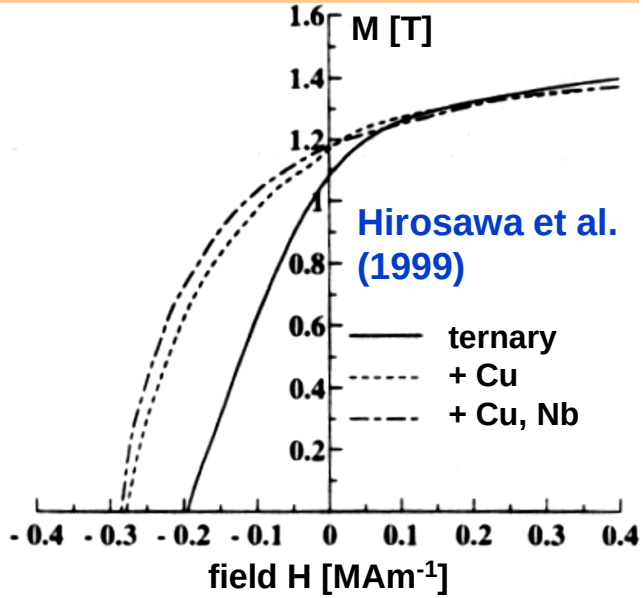

Demagnetisation recoil loops

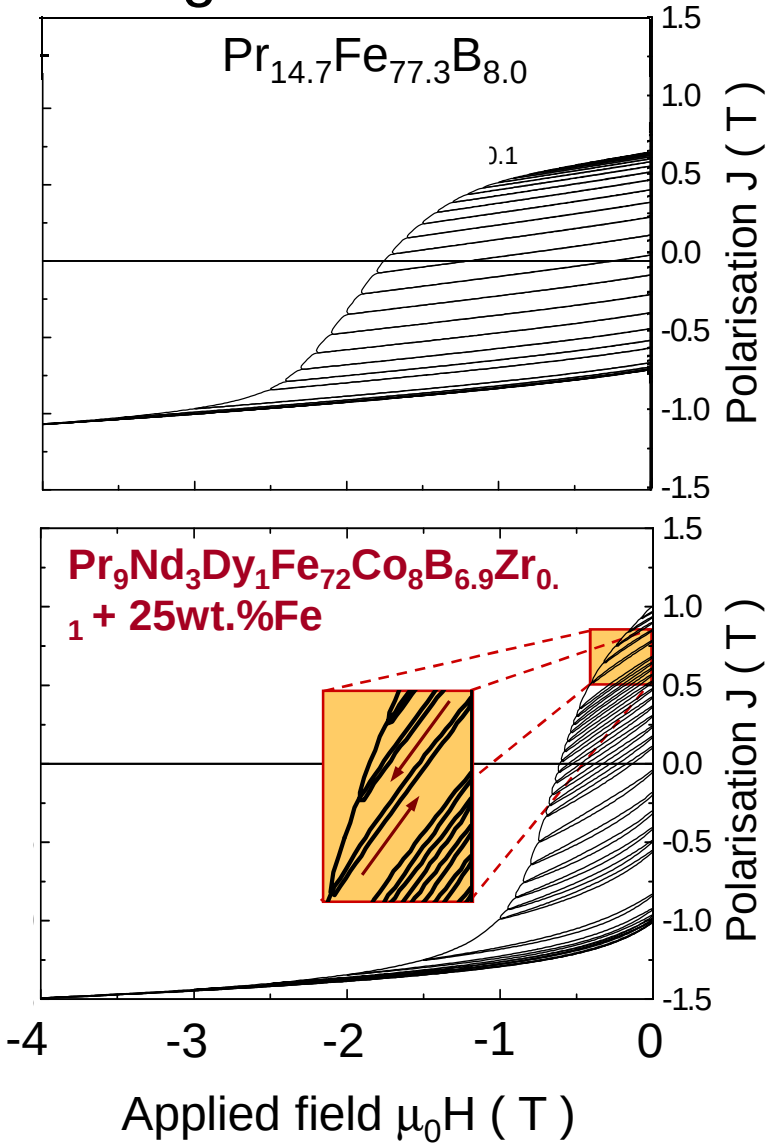

decoupled magnet

- $J_r / J_s \leq 0.5$ (but very large coercivity)
- closed recoil loops

exchange-coupled nanocomposite magnet

- magnetically single-phase behaviour
- open recoil loops
- high recoil permeability

reversible rotation of the exchange-coupled soft phase (**exchange-spring mechanism**)

A. Bollero, PhD TU Dresden

Ball milling technique

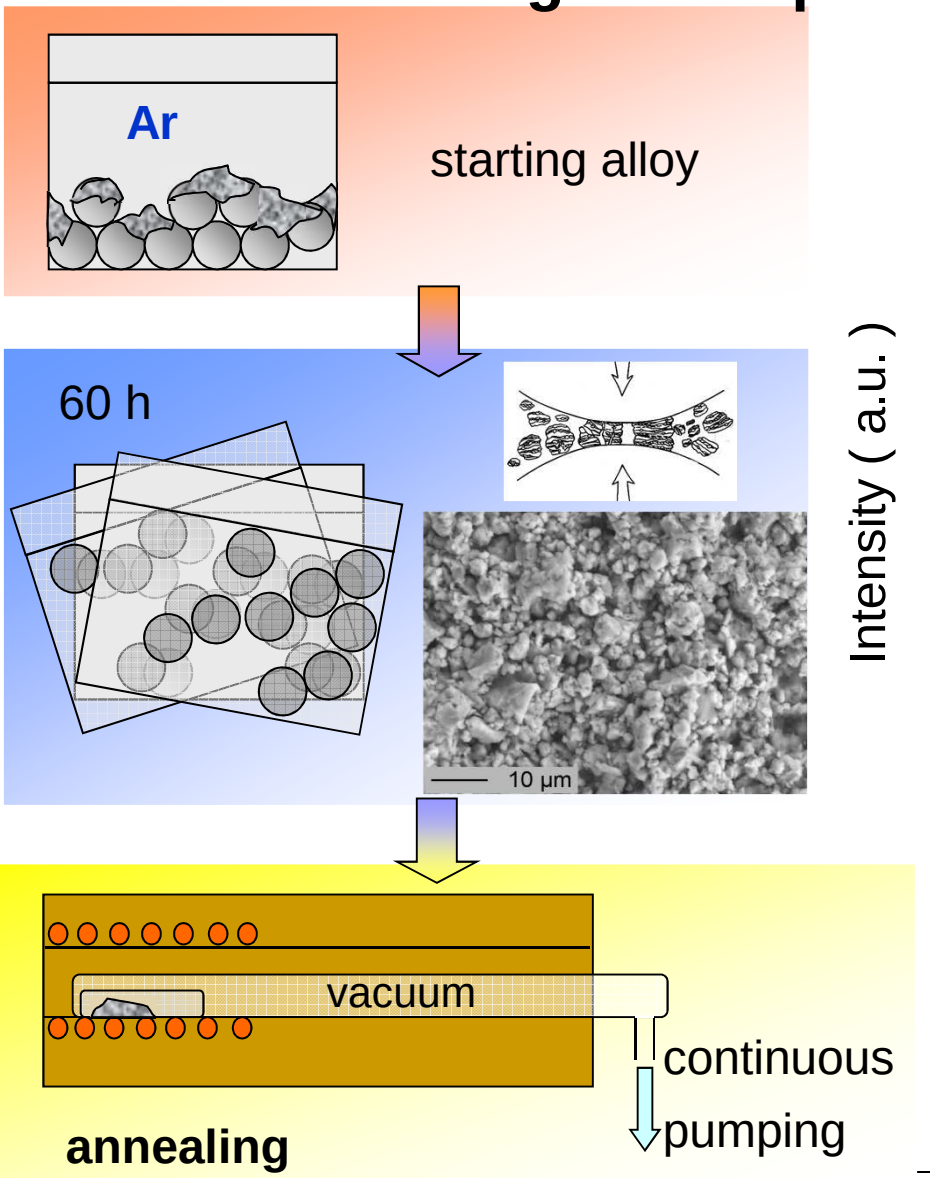

PrNdDyFeCoBZr

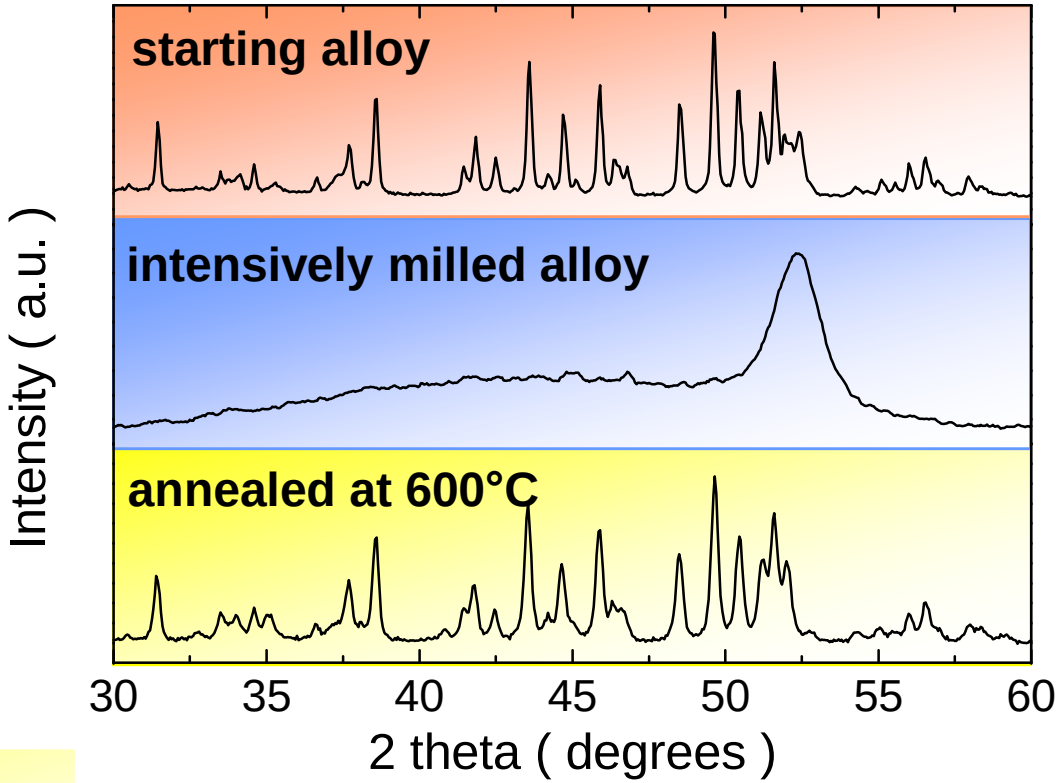

oxidation levels:
- **milled samples: < 0.3 wt.%**
- **milled + annealed: < 0.5 wt.%**

Isotropic intensively milled (Pr,Nd)FeB-type magnets

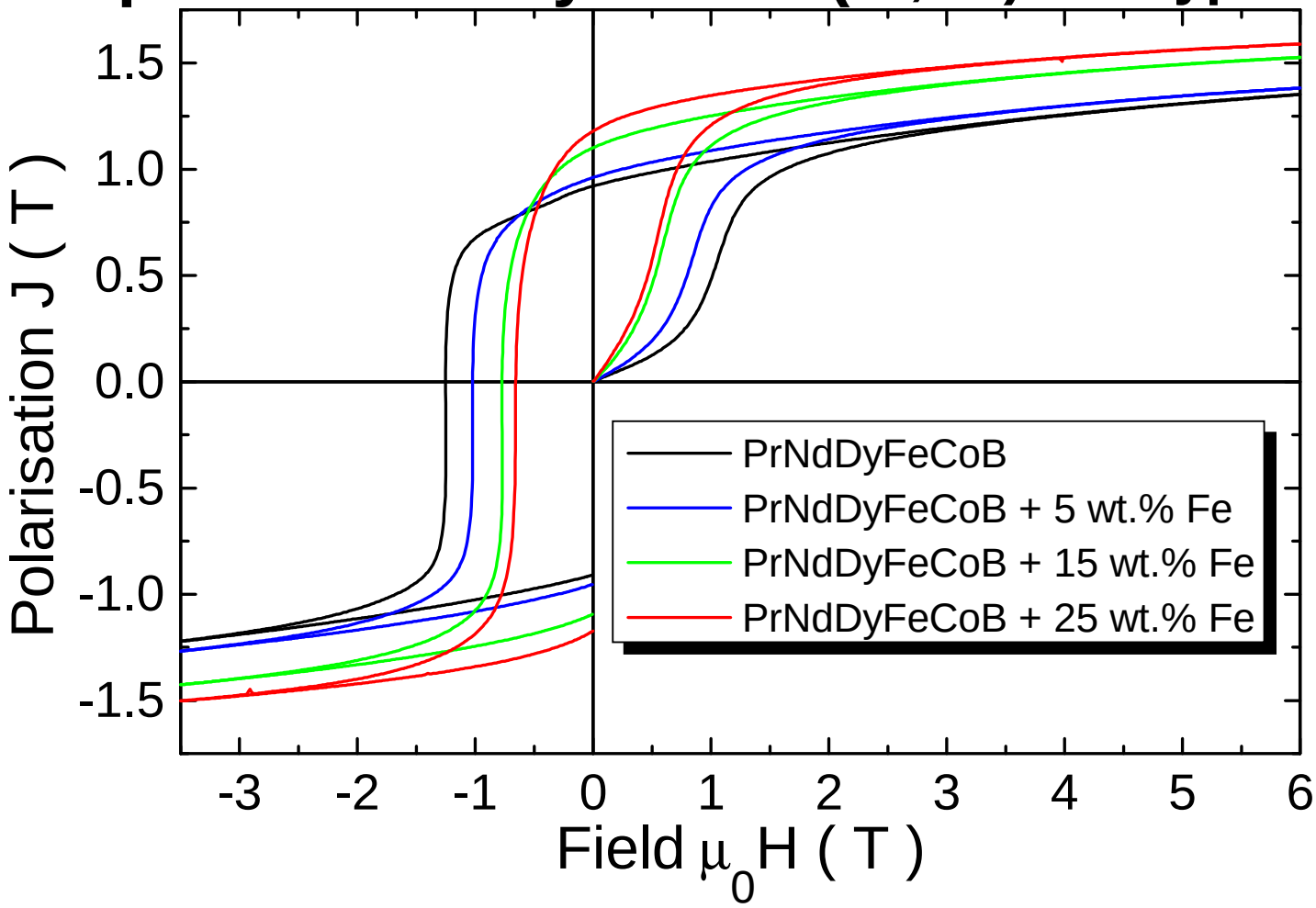

$R_{13}T_{80}B_7$

+

Dy & Zr

Co

$T_C \approx 380°C$

$_iH_c$ ↑

SAMPLE	remanence (T)	coercivity (T)	$(BH)_{max}$ (kJm^{-3})
$Pr_9Nd_3Dy_1Fe_{72}Co_8B_{6.9}Zr_{0.1}$	0.92	1.25	139
$Pr_9Nd_3Dy_1Fe_{72}Co_8B_{6.9}Zr_{0.1}$ + 5 wt.% Fe	0.96	1.02	149
$Pr_9Nd_3Dy_1Fe_{72}Co_8B_{6.9}Zr_{0.1}$ + 15 wt.% Fe	1.10	0.77	170
$Pr_9Nd_3Dy_1Fe_{72}Co_8B_{6.9}Zr_{0.1}$ + 25 wt.% Fe	**1.19**	**0.66**	**178**

Two-phase nanocomposite magnets

Schematic one-dimensional model of the micromagnetic structure of an **exchange-coupled composite material**:

E. F. Kneller and R. Hawig, IEEE Trans. Magn. **27**, 3588 (1991)

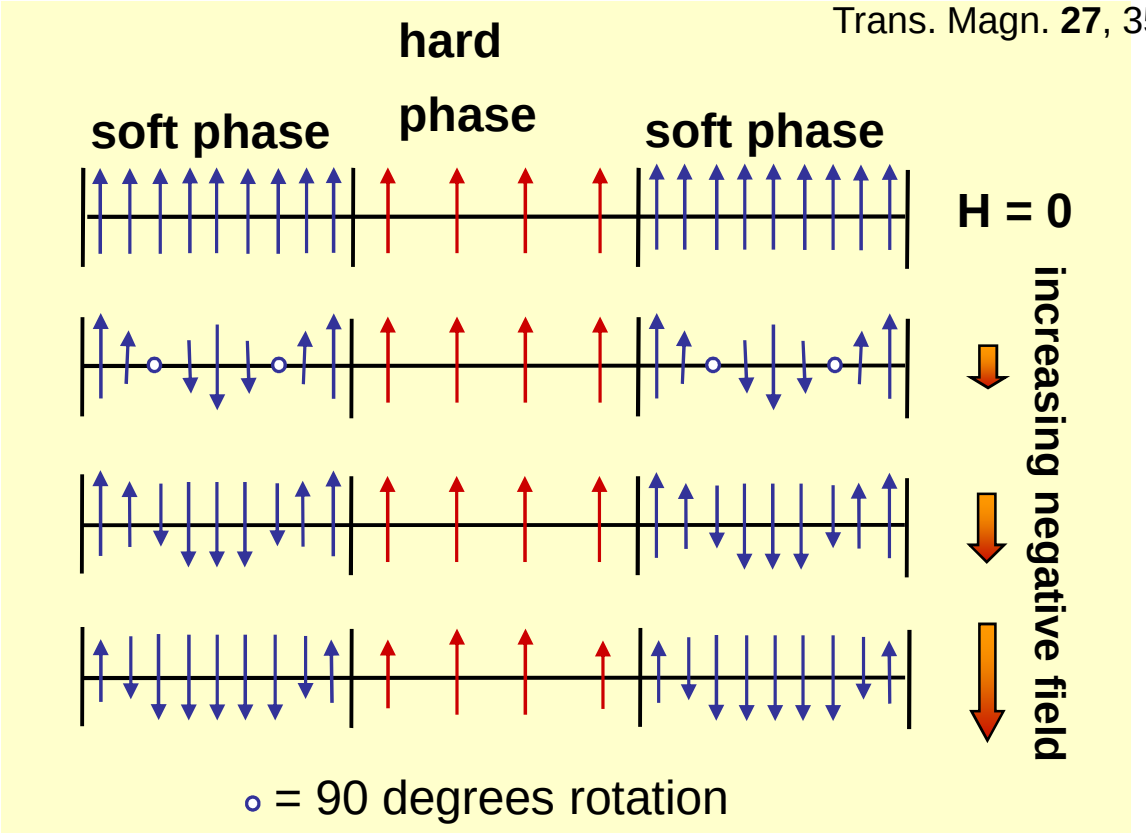

optimum grain size of soft phase ≈ $2\delta_w$ [hard phase]

the exchange fields from nearest neighbouring hard grains situated at both sides just fully cover the soft grain ⇒ exchange hardening of the soft grain

Wohlfarth's relation $J_r^d(H_m) = J_r - 2J_r(H_m)$

$J_r^d(H_m)$ for an assembly of magnetically **non-interacting** uniaxial single-domain particles

$\boldsymbol{J_r^d(H_m)}$: remanence after application of a reverse field, $-H_m$, to a saturated sample

$\boldsymbol{J_r}$: remanence measured after saturation ($H_m \rightarrow \infty$)

$\boldsymbol{J_r(H_m)}$: remanence after application and removal of the maximum field H_m to a <u>thermally demagnetised sample</u>

E. P. Wohlfarth, Advan. Phys. **8**, 87 (1959)

Nanocomposite magnet

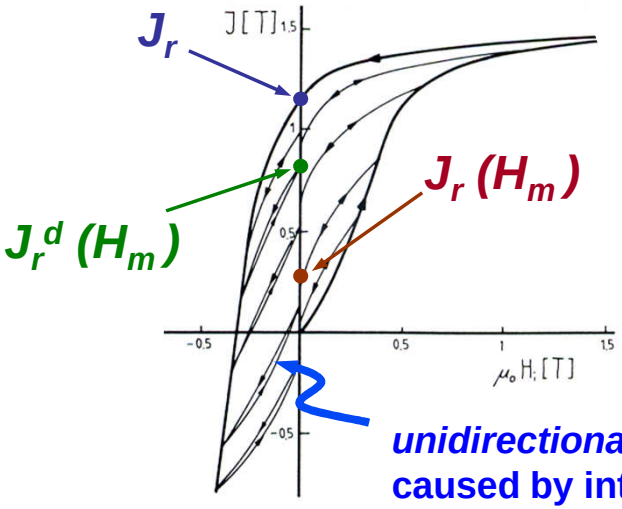

unidirectional anisotropy **caused by intergrain coupling**

$Nd_2Fe_{14}B$ / Fe_3B

Henkel-plot:

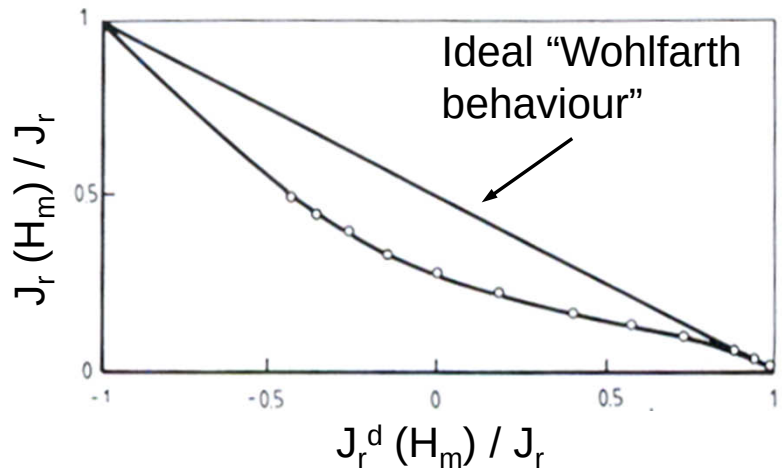

The deviation of $J_r^d(H_m)$ from Wohlfarth's relationship can be used for an interpretation of intergrain interactions

Recycling of rare earths

Global estimates of end-of-life recycling rates for 60 metals and metalloids (2008)

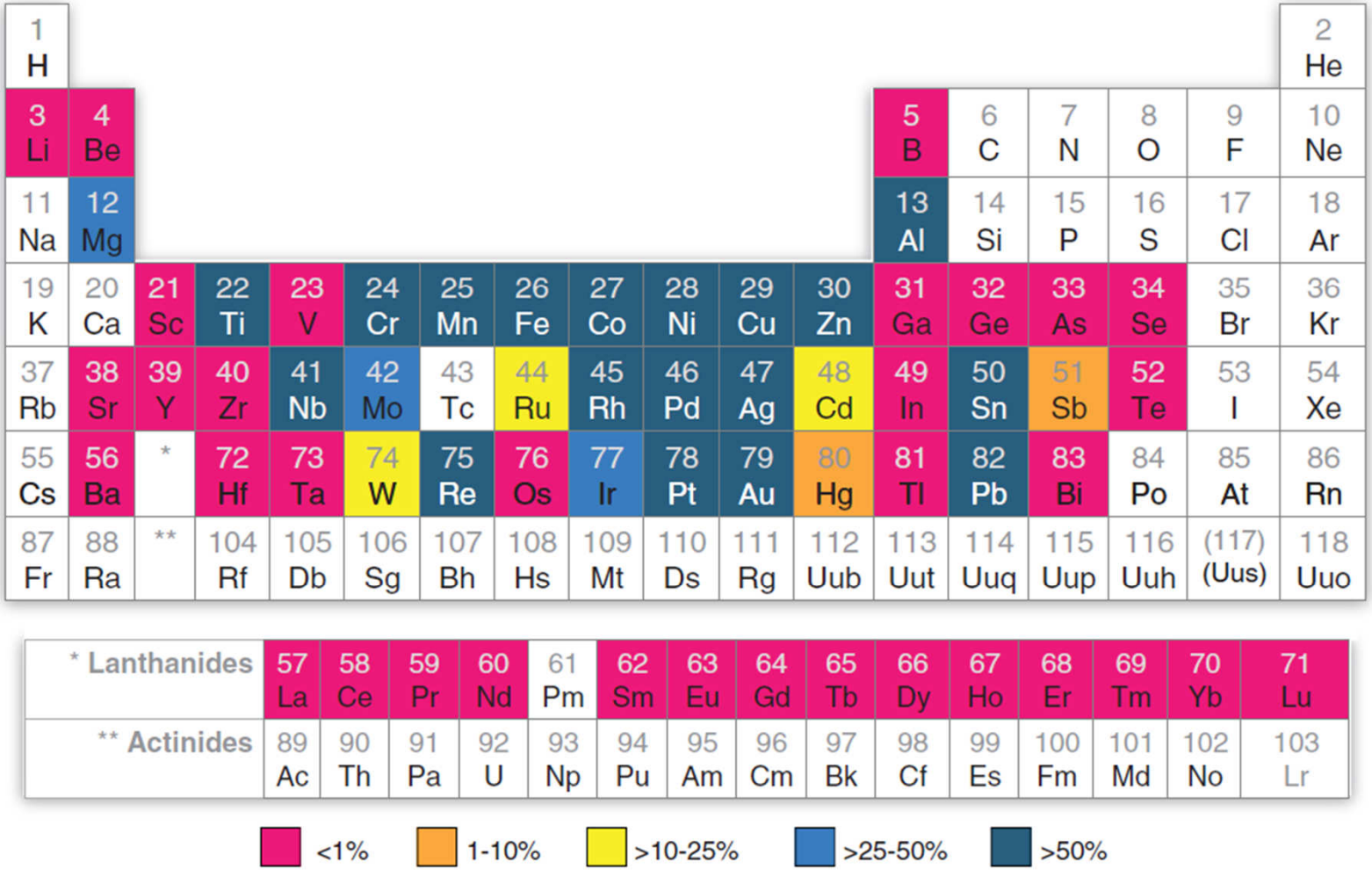

T. E. Graedel et al., J. Ind. Ecol. 15, 355 (2011).

Recycling by hydrogen processing

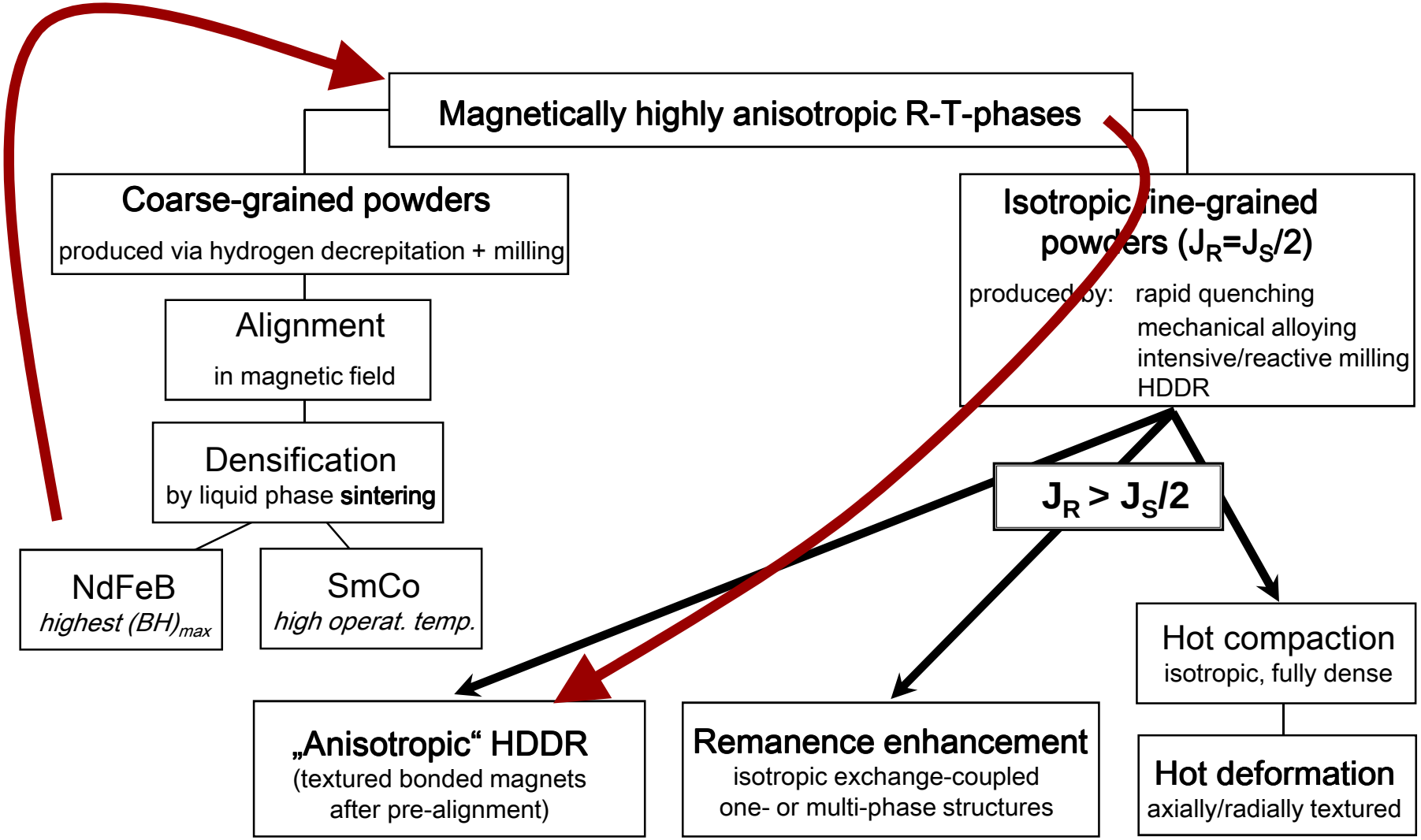

J. Phys. D: Appl. Phys. **33** (2000) R157

Hydrogen processing

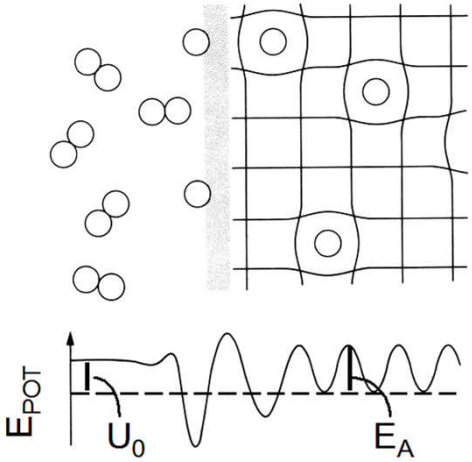

Schematic presentation of the gas-solid reaction*: dissociation* of molecular hydrogen at an interface, *penetration* and *diffusion* (interstitial solution) of hydrogen atoms in the bulk (the corresponding potential energy U_0 and the activation energy E_A are shown in the lower part).

0.3	0.88	0.77	0.70	0.66	0.64
H	**B**	**C**	**N**	**O**	**F**
2.20	2.04	2.55	3.04	3.44	3.98

***Covalent radii* in Å (top) and *electronegativities* (bottom) of light elements, which are candidates for use in interstitial modification. The atomic radius should be less than 1 Å but e.g. boron cannot easily be introduced by a low-temperature gas-solid reaction and the melting route is the preferred option. The high electronegativity of oxygen and fluorine on the other hand leads to an immediate disproportionation into oxides and fluorides rather than interstitial modification leaving H, C and N for gas-solid reactions**

Hydrogen processing

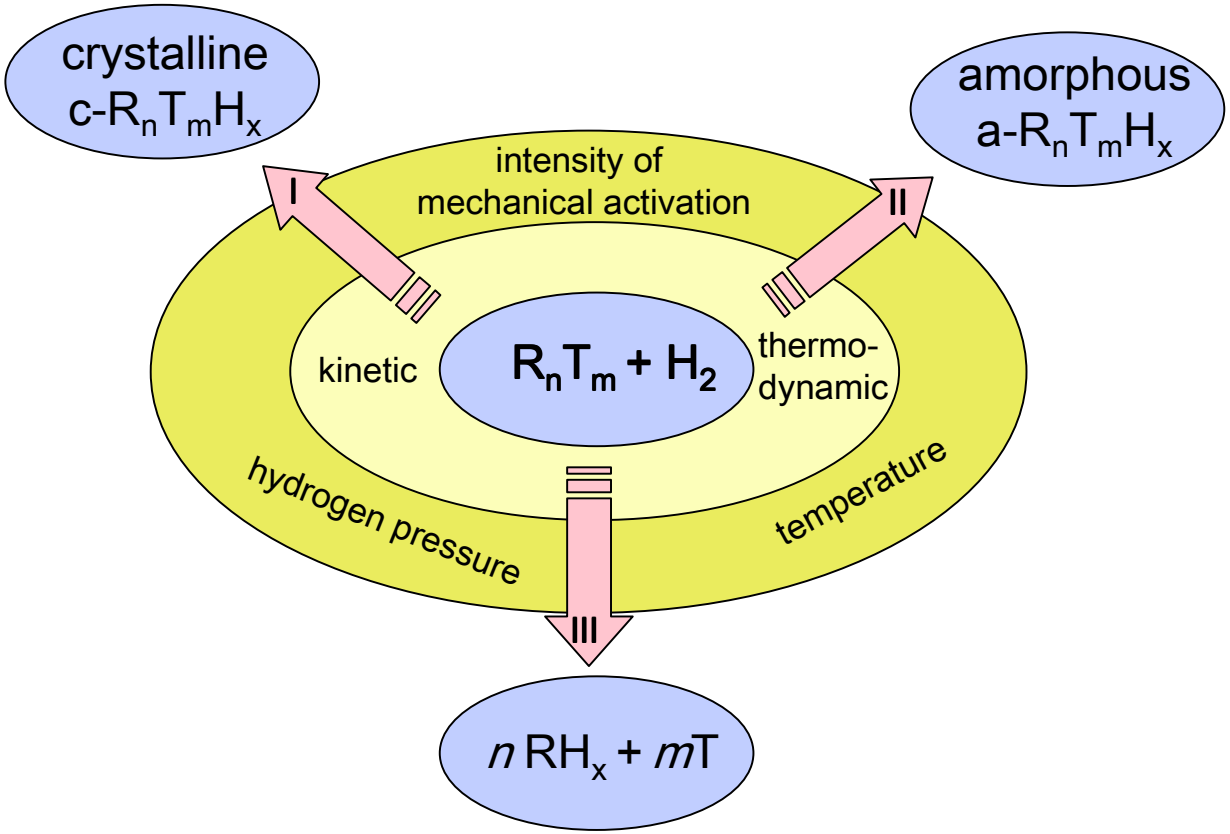

HDDR

$$Nd_2Fe_{14}B + \tfrac{1}{2}\,xH_2 \Leftrightarrow Nd_2Fe_{14}BH_x \pm \Delta H_1\,(HD)$$

$$Nd_2Fe_{14}B + (2\pm x)H_2 \Leftrightarrow 2NdH_{2\pm x} + 12Fe + Fe_2B \pm \Delta H_2$$

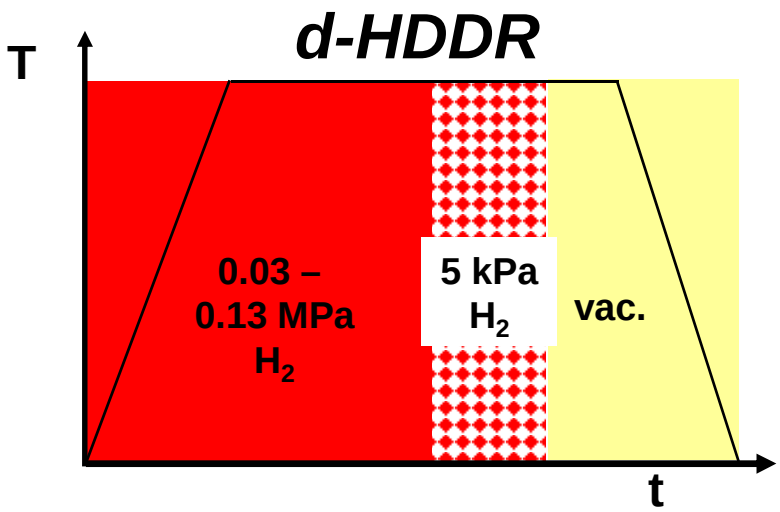

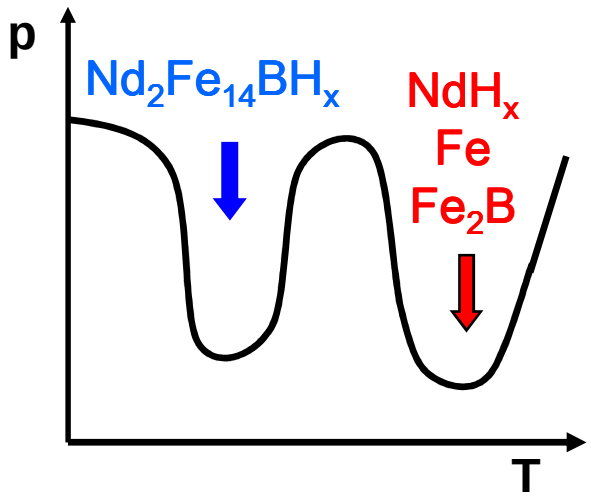

[1] T. Takeshita and R. Nakayama, "*Magnetic properties and microstructures of the NdFeB magnet powder produced by hydrogen treatment*", 10th Int. Workshop on RE Magnets..., Kyoto, Japan, 551 (1989).
[2] P. J. McGuiness, X. J. Zhang, X. J. Yin and I. R. Harris, "*Disproportionation in $Nd_{16}Fe_{78}B_6$ –type hydrides*", J. Less-Common Metals **158** (1990) 379.
[3] O. Gutfleisch, K. Khlopkov, A. Teresiak, K.H. Müller, G. Drazic, C. Mishima and Y. Honkura, IEEE Trans. on Magn. **39** (2003) 2926.

RECYCLING PROCEDURE

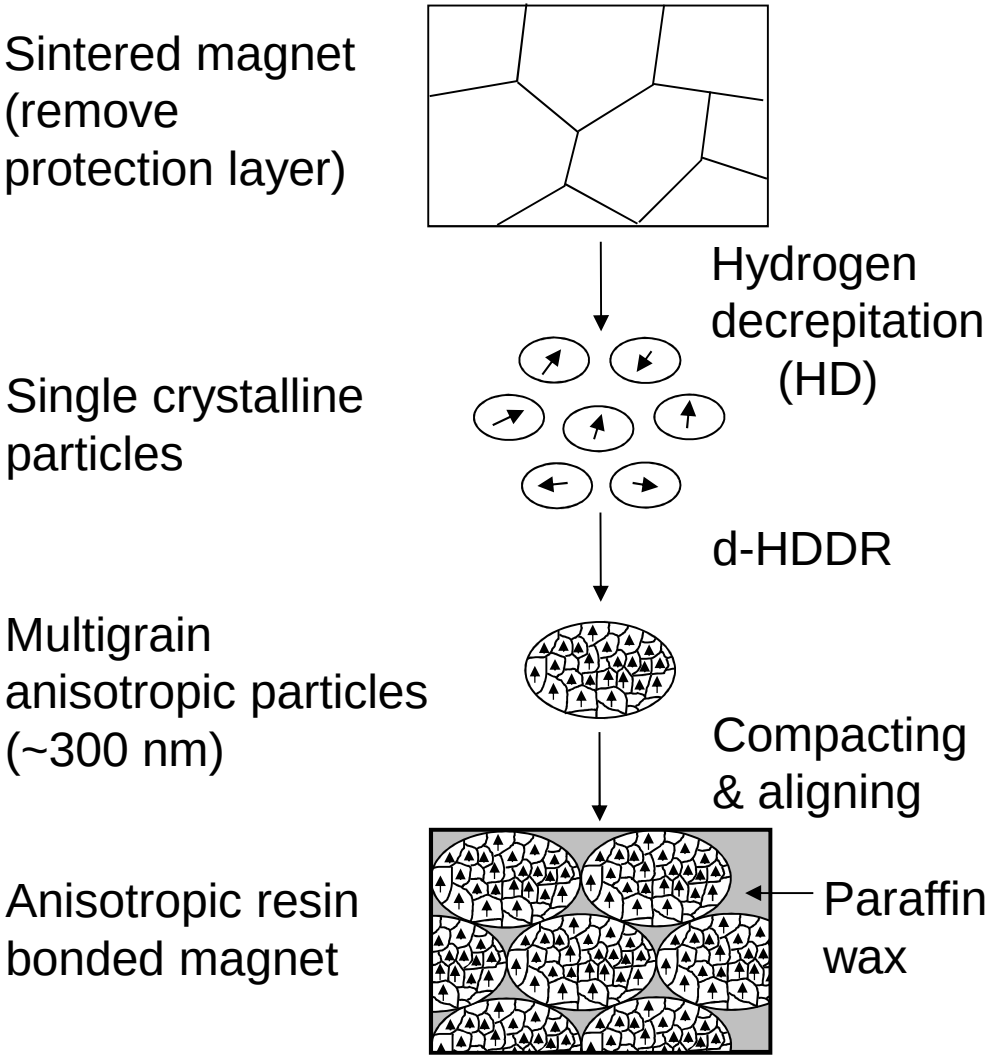

Adv. Energy Mat. 2012